



HAL
open science

The Pre-Obduction to Post-Obduction Evolution of the Sivas Ophiolite (Turkey) and Implications for the Precollisional History of Eastern Anatolia

Etienne Legeay, Geoffroy Mohn, Jean-Paul Callot, Jean-claude Ringenbach,
Alexey Ulianov, Kaan Sevki Kavak

► **To cite this version:**

Etienne Legeay, Geoffroy Mohn, Jean-Paul Callot, Jean-claude Ringenbach, Alexey Ulianov, et al.. The Pre-Obduction to Post-Obduction Evolution of the Sivas Ophiolite (Turkey) and Implications for the Precollisional History of Eastern Anatolia. *Tectonics*, 2019, 38 (6), pp.2114-2141. 10.1029/2018TC005114 . hal-02377191

HAL Id: hal-02377191

<https://hal.science/hal-02377191>

Submitted on 20 Jun 2024

HAL is a multi-disciplinary open access archive for the deposit and dissemination of scientific research documents, whether they are published or not. The documents may come from teaching and research institutions in France or abroad, or from public or private research centers.

L'archive ouverte pluridisciplinaire **HAL**, est destinée au dépôt et à la diffusion de documents scientifiques de niveau recherche, publiés ou non, émanant des établissements d'enseignement et de recherche français ou étrangers, des laboratoires publics ou privés.

Tectonics

RESEARCH ARTICLE

10.1029/2018TC005114

Key Points:

- The Sivas Ophiolite consists of a pre-obduction magma-starved ophiolitic sequence which formed in a suprasubduction setting during the Late Cretaceous
- The post-obduction sedimentary succession is characterized by Maastrichtian-Paleocene carbonate platform followed by clastic sediments reworking Tauride platform and Sivas ophiolite
- Shortening initiated during early Eocene along the southern edge of the Sivas Basin

Supporting Information:

- Supporting Information S1

Correspondence to:

E. Legeay,
etienne.legeay@univ-pau.fr

Citation:

Legeay, E., Mohn, G., Callot, J.-P., Ringenbach, J.-C., Ulianov, A., & Kavak, K. S. (2019). The pre-obduction to post-obduction evolution of the Sivas ophiolite (Turkey) and implications for the precollisional history of Eastern Anatolia. *Tectonics*, 38. <https://doi.org/10.1029/2018TC005114>

Received 25 APR 2018

Accepted 10 MAY 2019

Accepted article online 23 MAY 2019

The Pre-Obduction to Post-Obduction Evolution of the Sivas Ophiolite (Turkey) and Implications for the Precollisional History of Eastern Anatolia

Etienne Legeay^{1,2} , Geoffroy Mohn³, Jean-Paul Callot¹, Jean-Claude Ringenbach², Alexey Ulianov⁴, and Kaan Sevki Kavak⁵

¹E2S UPPA CNRS/TOTAL/University of Pau and Pays Adour, Laboratoire Des Fluides Complexes Et Leurs Reservoirs-IPRA, UMR5150, Pau, France, ²Structural Geology Department, Total SA, CSTJF, Pau, France, ³Géosciences Environnement Cergy, Université de Cergy-Pontoise, Cergy-Pontoise, France, ⁴Institut des Sciences de la Terre, Université de Lausanne, Lausanne, Switzerland, ⁵Department of Geological Engineering, Sivas Cumhuriyet University, Sivas, Turkey

Abstract The Anatolian block preserves remnants of Tethyan oceanic basins consumed by north dipping subduction zones until the Late Cretaceous prior to Paleogene collision. The Sivas Basin, which belongs to the Maastrichtian to Cenozoic Central Anatolian basins, is located in a key position limited to the north and the south by respectively the Pontides and Tauride ophiolitic bodies and to the west by the Kırşehir block. This study focuses on the southern margin of the Sivas Basin, where an obducted ophiolite is capped by Maastrichtian-Paleocene sediments. We present new field observations, with U-Pb zircon dating on magmatic rocks and geochemical analyses to (1) unravel the pre-obduction nature and origin of the ophiolitic basement and (2) describe the post-obduction tectonosedimentary evolution. The pre-obduction evolution shows that (i) the Sivas ophiolite is characterized by serpentinized peridotites, with minor magmatic intrusions, (ii) the top of the serpentinized mantle is characterized by a cataclastic deformation with ophicalcites interpreted as an extensional detachment fault, (iii) the U-Pb zircon dating of two magmatic intrusions yield age of 91.49 ± 0.8 Ma and 72.7 ± 0.5 Ma, and (iv) petrological and geochemical data show that the magmatic intrusions were affected by hydrothermal metamorphism. These data suggest that the Sivas ophiolite may have recorded forearc hyperextension in frame of a Late Cretaceous suprasubduction zone. The post-obduction evolution is characterized by the deposition of a Maastrichtian-Paleocene carbonate platform on the ophiolite, followed by clastic sediments containing reworked ophiolitic and Tauride Mesozoic clasts.

1. Introduction

The Anatolian plate documents the complex amalgamation of Gondwana-derived continental fragments from the Paleozoic onward, delimited by distinct suture zones, along the southern Eurasian margin (Figure 1; e.g., Okay, 2008; Robertson et al., 1996; Şengör & Yılmaz, 1981). These suture zones record the complex spatial and temporal closure of different Tethyan oceanic domains, which consist of complex lithostratigraphic associations of ophiolite sequences and marine sediments (e.g., Dercourt et al., 1986; Parlak et al., 2013; Parlak et al., 2013; Ricou, 1971; Robertson, 2002; van Hinsbergen et al., 2016). In particular, the closure of the Neo-Tethyan oceanic domain lasting from the Early Jurassic to the Paleogene is well documented along the İzmir Ankara Erzincan Suture Zone (İAESZ). This suture can be followed across Turkey with an east-west trend (Figure 1), separating the southern Eurasian active margin, in the Pontides (Çelik et al., 2011; Göncüoğlu et al., 2003; Hässig et al., 2015; Okay & Altner, 2007; Parlak, Çolakoğlu, et al., 2013; Sarıfakıoğlu et al., 2009), from a passive margin sedimentary sequence preserved in the Anatolide-Tauride domain (Gutnic, 1979; Mackintosh & Robertson, 2009, 2012; Özgül, 1984; Poisson, 1977; Robertson et al., 2013).

The tectonic configuration becomes more complex in Central Anatolia where the Anatolide-Tauride domain is separated from the Pontides arc by an intermediate continental domain, Anatolide-derived, referred to as the Kırşehir block, rimmed and overlain by ophiolitic bodies (Figure 1; e.g., van Hinsbergen et al., 2016; Yılmaz et al., 2000). In the frame of this complex tectonic evolution, the origin, genesis, and evolution of the numerous ophiolitic bodies located in the vicinity of the Kırşehir block are of critical importance,

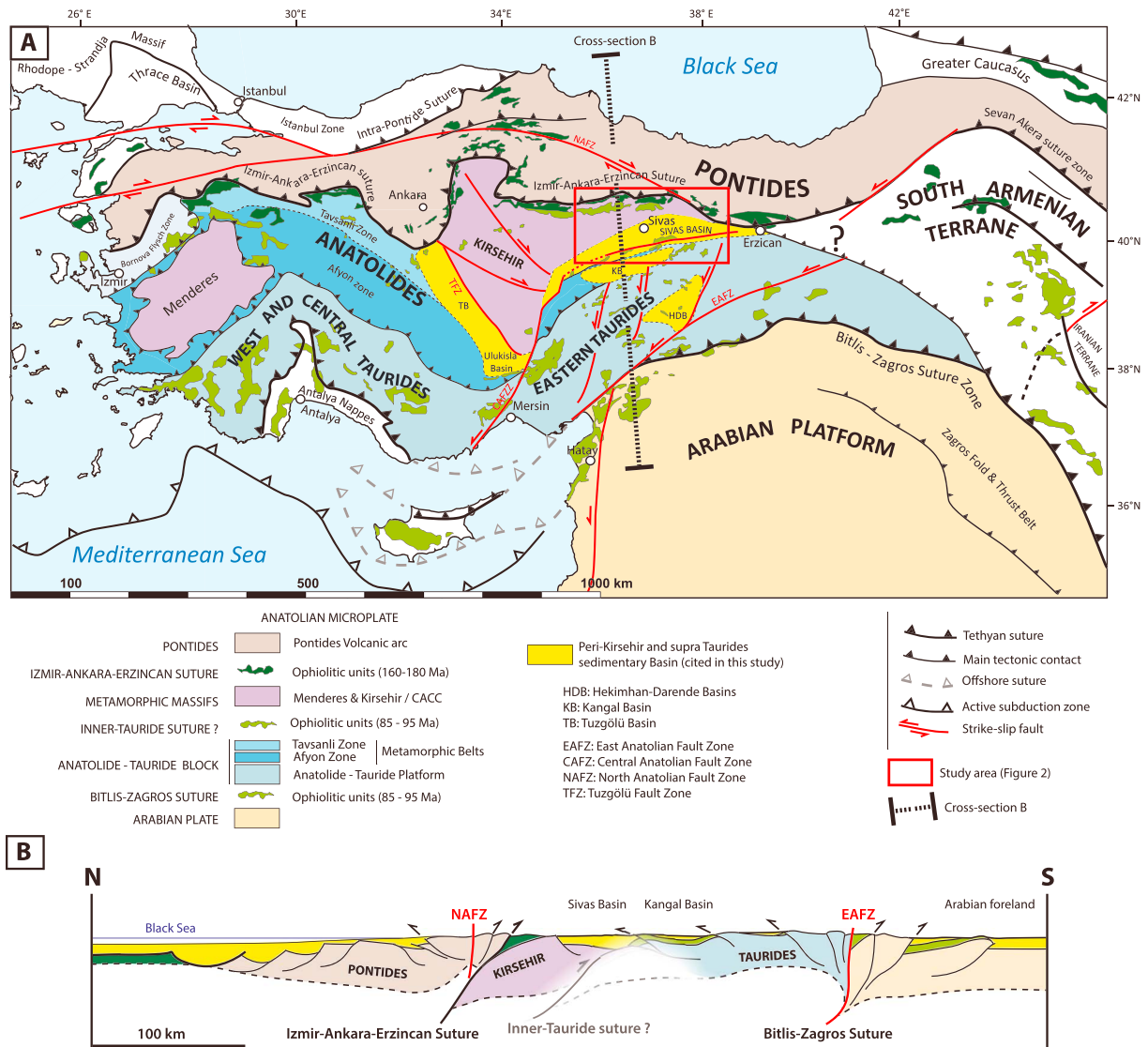


Figure 1. (a) Tectonic map of Turkey and Eastern Mediterranean region showing the major suture zones, faults systems, ophiolite-derived outcrops and tectonic units (modified from van Hinsbergen et al., 2016; Pourteau et al., 2013). The cited sedimentary basins in this study, southward of the Kırşehir block and above the Tauride, are highlighted in yellow. (b) Synoptic crustal-scale cross-section highlighting relationships between crustal blocks, ophiolites and tertiary basins (simplified from Legeay, Pichat, et al., 2019).

especially at its eastern edge where it is tapering off. In particular, the eastern edge is characterized by the development of the Sivas Basin that recorded Maastrichtian to Pliocene sedimentary sequences (e.g. Gökten, 1983, Guezou et al., 1996, Poisson et al., 1996, Temiz et al., 1993). This basin lies over the Kırşehir block to the west, the İAESZ to the north, while to the south it covers an important ophiolitic body, referred to as the Sivas ophiolite (Figure 2; Guezou et al., 1996; Temiz, 1996). The evolution of this ophiolite remains poorly studied and was assigned either to the İAESZ (e.g. Poisson et al., 1996, Temiz, 1996) or to the Inner Tauride Suture Zone (ITSZ; e.g., Guezou et al., 1996; Kavak et al., 2017).

This study aims to fill data gaps on the Sivas ophiolite by investigating its pre-obduction to post-obduction evolution and its significance for the complex tectonic evolution of Central Anatolia. On the one hand, the Sivas ophiolite pre-obduction lithostratigraphic association, made essentially by serpentinized mantle with rare occurrence of mafic intrusive rocks, differs from the “Penrose ophiolite sequence” questioning its pre-obduction nature, age, and origin. On the other hand, its well preserved and developed post-obduction sedimentary record enables us to characterize the initial development of supraophiolitic sedimentary system.

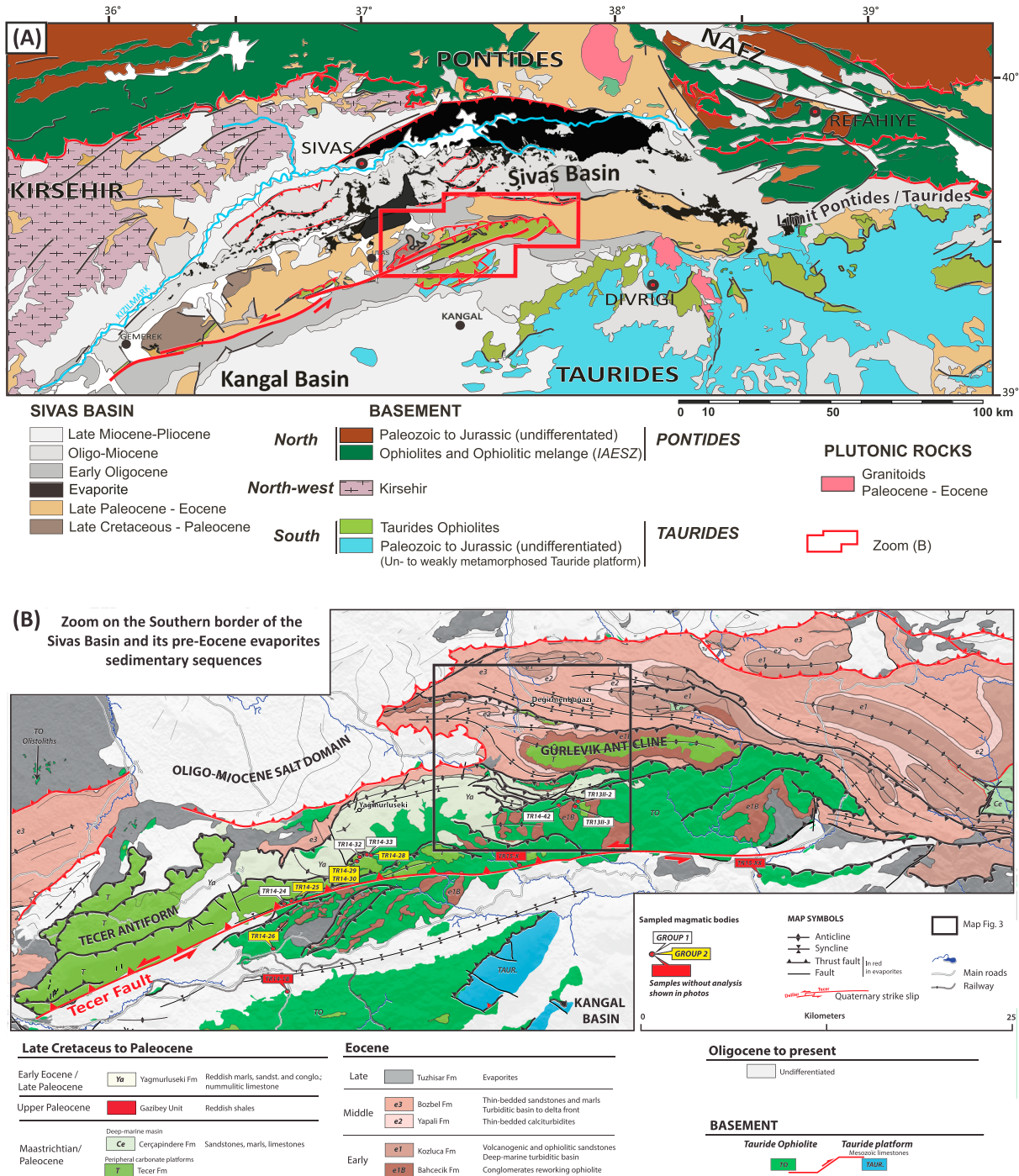


Figure 2. (a) Simplified geological map of the Sivas Basin showing main basement units and simplified stratigraphy. Geological data are compiled from Bilgic (2002) and Ribes et al. (2015). (b) Geological map of the Southern margin of the Sivas Basin after Legeay, Pichat, et al. (2019). The black square corresponds to Figure 3.

The pre-obduction evolution of the Sivas ophiolite is investigated through new structural, lithostratigraphic, and petrological observations combined with geochemical data and U-Pb zircon ages on the magmatic rocks. The detailed Late Cretaceous to early Paleogene post-obduction sedimentary sequences are associated with a first-order deformation calendar of the southern edge of the Sivas Basin. Eventually, these new data are integrated in the general geodynamic context of central Turkey.

2. Geological Setting

2.1. Regional Geodynamic Setting

The geology of Central Anatolia is characterized by distinct sutures zones that border several crustal blocks (Figure 1). To the north, the Pontides represent an E-W trending fold and thrust belt considered as the Southern Eurasian active margin during the Mesozoic (Okay & Nikishin, 2015; Şengör & Yılmaz, 1981; Ustaömer & Robertson, 2010). The Pontides are bounded to the south by the İAESZ (Figure 1). This suture marks the closure of the northern branch of the Neo-Tethys Ocean during the Late Cretaceous to early Paleogene (e.g., Şengör & Yılmaz, 1981). The İAESZ is bounded to the south by the Kırşehir Block, of continental origin. Paleomagnetism evidence documents that the Kırşehir Block was elongated along a N-S trend during Late Cretaceous (Lefebvre et al., 2013), westward of the present-day Eastern Tauride (Gürer et al., 2016; van Hinsbergen et al., 2016). The Kırşehir block was bounded to the east by the “Eastern Kırşehir Fracture Zone” (EKFZ), forming the limit of an oceanic domain during the Paleogene between Pontides and Eastern Tauride as proposed in recent reconstructions (Gürer, Plunder, et al., 2018).

The Kırşehir block suffered a Barrovian-type metamorphism during the Late Cretaceous (Whitney et al., 2001), related to a regional burial below an oceanic lithosphere as shown by relicts of ophiolitic melange and obducted suprasubduction zone ophiolite fragments (Lefebvre et al., 2011; van Hinsbergen et al., 2016; Yalınız et al., 2000). To the south, the Kırşehir Block is in tectonic contact with the Tauride-Anatolide Platform in Central Anatolia. Along this contact, numerous ophiolitic bodies have been described and referred hereafter as the Tauride ophiolites (Dilek et al., 1999; Parlak, Karaoğlan, et al., 2013). These ophiolites were obducted and emplaced over the Tauride-Anatolide domain during the Campanian-Maastrichtian (Dilek et al., 1999; Parlak, Karaoğlan, et al., 2013; Poisson et al., 2016; Robertson, 2002). They are generally characterized from bottom to top by an ophiolitic mélange, a metamorphic sole, and an ophiolitic sequence, consisting among others of variably serpentinized and deformed peridotites, mafic intrusive, and extrusive rocks (Parlak et al., 2006; Parlak, Karaoğlan, et al., 2013). The significance of these Tauride ophiolites has been the subject of long-standing debates. They have been interpreted either as a separate suture zone (i.e., the Inner Tauride Suture Zone, ITSZ), representing a branch of the Neo-Tethyan system (Görür et al., 1984; Menant et al., 2016; Robertson et al., 2012; Şengör & Yılmaz, 1981) or attached to the İAESZ belonging therefore to the same oceanic domain than the ophiolites located to the north of the Kırşehir Block (Lefebvre et al., 2013; Maffione et al., 2017; Poisson et al., 1996; van Hinsbergen et al., 2016). Southward, the Tauride-Anatolide block represents a continental domain, classically divided in two units (Pourteau et al., 2010; Robertson et al., 1991; Şengör & Yılmaz, 1981): (1) to the north, the Anatolide (Afyon and Tavşanlı zones, Menderes Massif) affected by Late Cretaceous to Early Cenozoic compressional deformation and metamorphism (e.g., Gürer, Plunder, et al., 2018; Plunder et al., 2015) and (2) to the south, the unmetamorphosed passive margin sedimentary sequence of the south verging Tauride fold-and-thrust belt (e.g., Parlak, Metin, et al., 2013; Robertson, Parlak, Ustaömer, et al., 2013; Figure 1). During late Eocene to Miocene, the Tauride recorded a compressional stage that propagated from south to north, caused by closure of southern Neotethys and Arabia-Eastern Tauride collision. This stage is highlighted in Taurides by north verging thrusts representing the retroforeland of this collisional zone (e.g. Darin et al., 2018, Kaymakçı et al., 2010).

2.2. Geological Setting of the Sivas Basin

The Sivas Basin is located at the interface between distinct tectonic domains (Figure 2a): The northwestern margin is represented by the Kırşehir Block, the northern margin by ophiolites and ophiolitic mélanges belonging to the İAESZ and Pontides, and the southern margin by an ophiolitic massif referred to as the Sivas ophiolite structurally over the Tauride (Guezou et al., 1996; Kurtman, 1973; Poisson et al., 1996; Temiz et al., 1993). Poisson et al. (2016) date the obduction of the Sivas ophiolite over the Tauride between late Santonian and pre-late Campanian, using the biostratigraphic content of overlying and underlying sedimentary formations.

Past studies have described the stratigraphic succession of the southern margin of the Sivas Basin above the ophiolite (Aktimur et al., 1990; Artan & Sestini, 1971; Cater et al., 1991; Guezou et al., 1996; Poisson et al., 1996; Temiz, 1996). The oldest well-dated sedimentary formation (Figure 2b) consists of shallow-water carbonate platforms stratigraphically dated as Maastrichtian to Thanetian and deposited on top of the ophiolite. These platform facies are referred to as the Tecer Formation (İnan & İnan, 1990), passing northward to deep

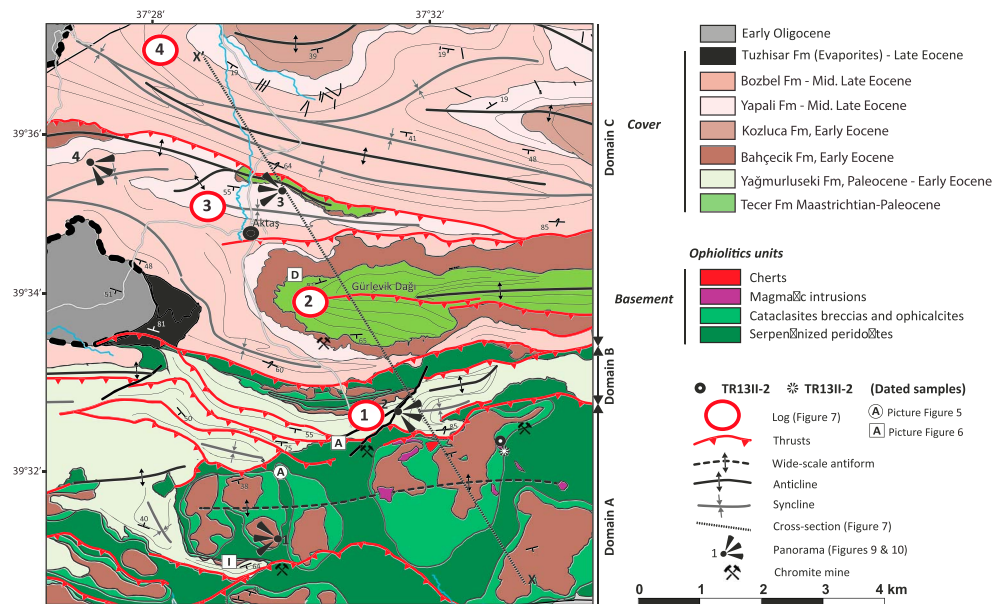


Figure 3. Detailed geological map of the study area near the Gürlevik anticline, at the southern edge of the Sivas Basin (location in Figure 2b). The trace of the cross section X-X' corresponds to the section in the Figure 7. Keys contacts shown in Figures 5 and 8 are located.

marine facies of the Çerpaçindere Formation (Aktimur et al., 1990). The late Paleocene to Eocene succession (see review of Legeay, Pichat, et al., 2019) is mainly represented by coarse clastic sediments composed of detritic discharge along the southernmost border (Yağmurluseki and Bahçecik Formations) that pass northward to basinal deposits until the middle to late Eocene (Kozluca, Yapalı, and Bozbel Formations). The latest Eocene to Oligocene deposits record the transition from marine to continental depositional environments associated with sedimentation of widespread evaporitic sequences (Figure 2b). The post-Oligocene evolution of the Sivas Basin is characterized by important salt tectonic activity well developed in its central and northern parts (Callot et al., 2014; Kergaravat, 2016; Kergaravat et al., 2013; Kergaravat et al., 2017; Legeay, 2017; Legeay, Pichat, et al., 2019; Legeay, Ringenbach, et al., 2019; Pichat, 2017; Pichat et al., 2016; Pichat et al., 2018; Ribes, 2015; Ribes et al., 2015; Ribes et al., 2016; Ribes et al., 2018; Ringenbach et al., 2013).

3. Methods

This study is based on a multidisciplinary approach combining structural, stratigraphic, and petrographic investigations, as well as geochemical analyses and U-Pb zircon geochronology. In particular, we focused on the mafic intrusive rocks emplaced within the serpentinized mantle along the southern edge of the Sivas Basin. Field work enables us to characterize the main lithostratigraphic association of the ophiolitic sequence. The geological maps shown in Figures 2 and 3 are based on outcropping geological units mapped in the field with the support of orthophotographs provided by GoogleEarth®. During fieldwork, compass clinometers or Fieldmove® software (Midland Valley) were used to collect structural and dip data.

Analytical methods and protocols for geochemistry and U-Pb zircon dating are shown in supporting information Text S1. Petrographic observations were realized in the field and subsequently confirmed by thin section analyses. Selected pictures are shown in section 4.3. Rock type has been identified based on estimated modal proportion completed with Nb/Y versus Zr/TiO₂x0.0001 (after Winchester & Floyd, 1977) and Th versus Co (after Hastie et al., 2007) diagrams provided in Supplementary Material 2.

Thirteen samples of magmatic rocks were selected for geochemical analyses (section 5) from Tecer to Gürlevik Mountain anticlines (locations of samples are shown in Figure 2b). The samples were selected for the representativeness of observed lithologies and their apparent low degree of alteration.

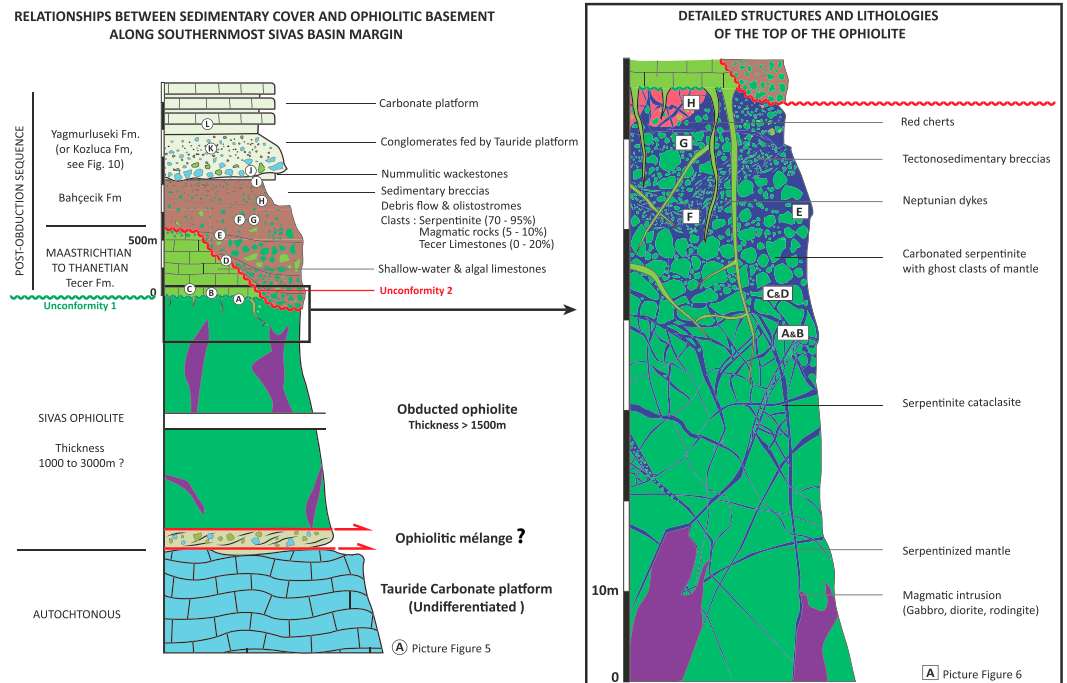


Figure 4. General and detailed “lithostratigraphic” sections across the study area. The detailed “lithostratigraphic” section shows the main lithologies and structures at the top of the ophiolitic unit as well as the overlying Maastrichtian to early Eocene sedimentary sequences. The location of the photographs shown in Figures 5–11 is indicated by squares and circles.

Despite careful mineral separations, only two samples contained zircons that eventually were dated by U-Pb zircon techniques (section 6). Radiogenic ratios for U-Pb dating are presented in supporting information Text S4.

4. The Lithostratigraphy and Structure of the Sivas Ophiolite

The Sivas ophiolite forms a large NE-SW trending body about 90-km long and 5-km wide located at the southern boundary of the Sivas Basin, between the Gürlevik/Tecer Mountains to the north and the Tauride carbonate platform to the south (Figure 2b). In particular, the tectonosedimentary relationships between the ophiolitic basement and the sedimentary cover are well exposed along the southern border of the basin in the Gürlevik Mountain area (Figure 3). It is composed of different lithologies ranging from ultramafic/mafic rocks to sedimentary rocks that will be described in the following sections (Figure 4).

4.1. Serpentinized Mantle Peridotites

The Sivas “ophiolite” consists essentially of strongly serpentinized (70%–90% serpentinization in average) spinel harzburgite and subordinate lherzolite and dunite (Figures 4 and 5). Despite the strong serpentinization, the original texture is locally preserved. Olivine and orthopyroxene are generally completely replaced by serpentine showing typical mesh, hourglass, and bastitic textures. Cr-spinel is often well preserved showing a red to dark brown color associated with euhedral to subhedral shape with millimeter-sized grains in thin sections. Furthermore, dunite is associated with abundant chromite deposits all over the Sivas ophiolite. No clear evidence for pelagic sediments or even extrusive magmatism, such as pillow basalts, were observed over the serpentinized mantle. Locally siliceous red cherts are present at the top of the mantle (Figures 4 and 5); however, no radiolarian fauna have been recognized in thin sections. Therefore, these red cherts are likely the product of chemical siliceous precipitation at the seafloor (e.g., Seibold & Berger, 2017). In addition, tectonic (Figures 5b–5d) to tectonosedimentary breccias (Figures 5e–5g), composed only of serpentinized mantle clasts and serpentine arenites of several meters thick, are observed directly overlying the mantle. However, their age and significance remain unclear.

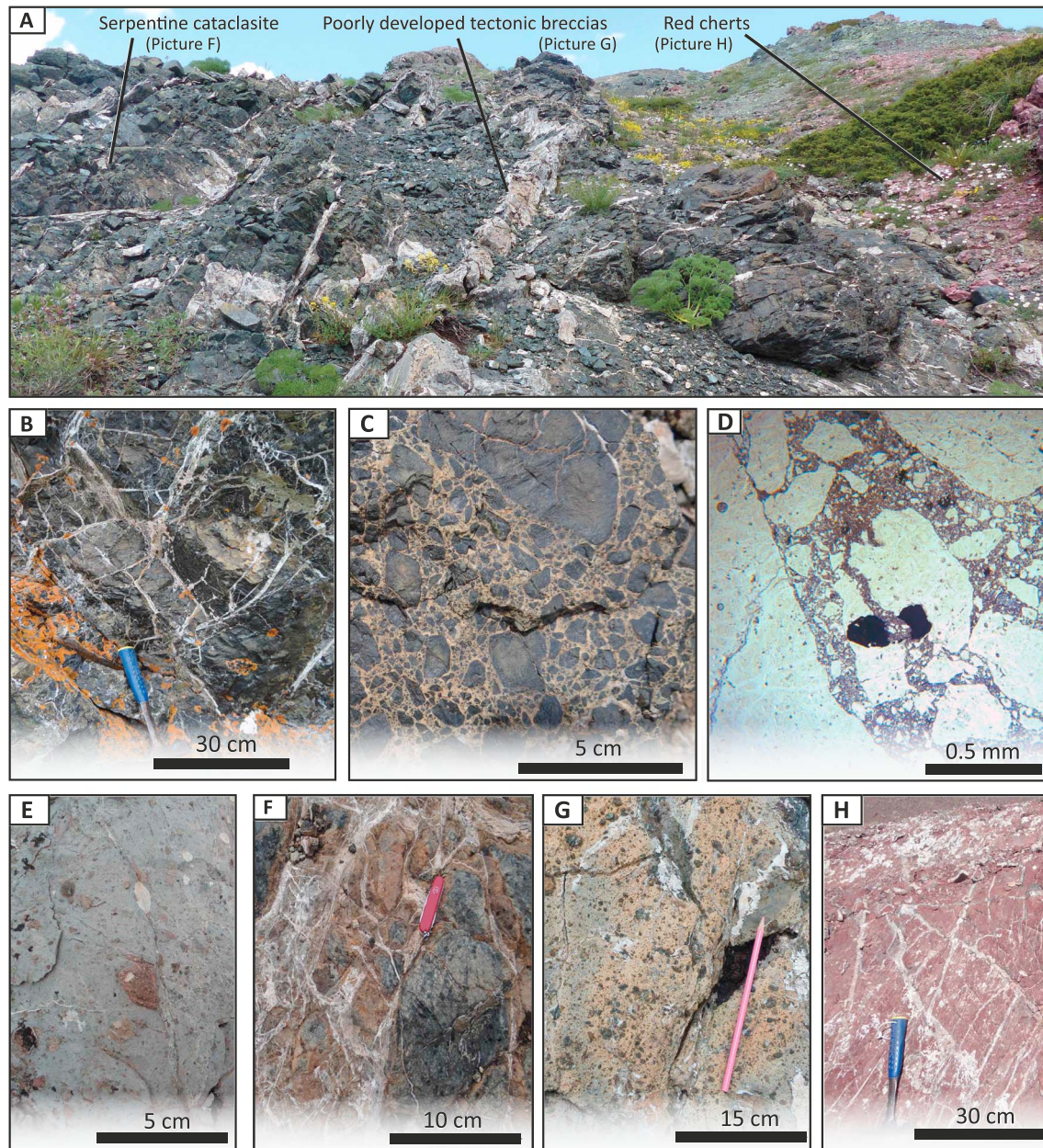


Figure 5. Photographs of structures and lithologies observed at the top of the serpentinized peridotite of the Sivas ophiolite. (a) Outcrop of the top of the mantle showing occurrences of serpentinite breccia associated with calcite veins and red cherts on the top. (b) Brecciated serpentinized mantle with calcite veins. (c) Serpentinite breccia. (d) Photomicrographs of serpentinite cataclasite showing a fractured spinel. (e) Serpentinite breccia associated with calcite veins (f) Ophicalcite with serpentine ghost clasts. (g) Ophicalcite made by calcite matrix with serpentine clasts. (h) Red cherts with calcite veins observed locally at the top of the peridotite.

4.2. Deformation Structures in the Peridotite

The top of the serpentinized peridotite is consistently characterized by cataclastic deformation associated with fluid circulation and ophicalcites. Along a vertical profile from the bottom to the top, the serpentinized mantle passes gradually to serpentinite cataclasites and breccias together with an increase of the intensity and distribution of serpentine and calcite veins (Figures 4 and 5). The cataclastic deformation is observed from a few meters to tens of meters below the top of the ophiolite.

The serpentinite breccias are generally clast-supported associated with angular to subangular shaped clasts (Figures 5c and 5d). The grain size is highly variable, ranging from micrometers to centimeters. Locally, a

more intense brecciation is observed, characterized by millimeter to micrometer clasts, embedded in a serpentine matrix. The brecciation is typically associated with a complex network of veining showing multiple generations with both straights and anastomosed geometries. The veins are filled either by serpentine or calcite with thickness ranging from mm to cm. The fractured serpentinized mantle documents a typical jigsaw-puzzle structure suggesting at least locally in situ fragmentation (Figure 5d).

The very top of the ultramafic body is characterized by a complex association of the serpentinite cataclasites with calcite veins (Figures 5e–5g) referred to as ophicalcite (for review, see Artemyev & Zaykov, 2010; Bogoch, 1987; Clerc et al., 2014; Lemoine et al., 1987). The strongly fractured serpentinized mantle is associated with an intense mesh of calcite-filled fractures, similar to the type 1 ophicalcite (OC1) of Lemoine et al., 1987 (Figures 5b and 5f). Locally ophicalcites are made of rounded to angular clasts of serpentinized peridotites (mm to dm), embedded in a fine-grained calcite to serpentine matrix (Figures 5e and 5g). In situ replacement of serpentinite by calcite is sometimes observed, while some peridotite clasts are crowned by calcites, suggesting important fluid circulation.

4.3. Mafic Intrusive Rocks

The serpentinized mantle from the Sivas ophiolite is intruded by isolated magmatic bodies that suffered extensive metamorphic recrystallizations. All the observed mafic bodies were emplaced within the serpentinized mantle, while no direct contact with the overlying sedimentary succession has been reported. The size of these magmatic bodies is highly variable. It consists mainly of small intrusions, metric to decametric in size, which form today small reliefs on the landscape at the surface of the serpentinized mantle. Locally rodingitized dykes are observed cutting across the serpentinized peridotites. In particular, two main magmatic gabbroic to dioritic bodies were observed within the Sivas ophiolite. The biggest one is located east of the Tecer Mountain (near Yağmurluseki village) with an approximate size of 2 km E-W and 1 km N-S. The other one, which is located south of the study area near Çavdar, has a diameter of 1 km.

In general, most of the magmatic rocks are now amphibolitized microgabbro, microdiorite made of plagioclase + green amphibole ± epidote ± chlorite (Figure 6). Despite the pervasive metamorphic overprint, original magmatic structures can be observed locally. Green amphibole contains rare clinopyroxene and brown amphibole inclusions, although the magmatic or metamorphic origin of the brown amphibole remains uncertain (Figure 6a). Euhedral to subhedral magmatic plagioclase is generally preserved (Figures 6a, 6c, and 6d). However, frequent fine-grained plagioclase + chlorite + sericite aggregates are interpreted as pseudomorphs of magmatic plagioclase. Locally, subordinate troctolite or pegmatitic gabbro can be found (Figures 6b and 6g, respectively). The medium-grained troctolite is composed of plagioclase + olivine ± clinopyroxene (Figure 6b). The pegmatitic gabbro is characterized by coarse-grained plagioclase + clinopyroxene, the latter being locally rimmed by secondary brown to green amphibole (Figure 6g). Most of the magmatic rocks are undeformed but present locally a weak fabric defined by the preferred orientation of secondary plagioclase and green amphibole (Figures 6c and 6d). All together, petrographic evidence indicates a strong recrystallization, approaching 80% to 90%, within the greenschist to amphibolite facies conditions, leading to an almost complete replacement of the primary magmatic assemblages.

5. Post-Obduction Maastrichtian to Middle Eocene Sedimentary Cover

Post-obduction Maastrichtian to middle Eocene sediments overlying the Sivas ophiolite are detailed in this section (modified from Legeay, Pichat, et al., 2019). They are characterized by strong lateral thickness and facies variations related to north verging thrust sheet emplacement (Figure 7).

5.1. Maastrichtian to Paleocene

The first well-identified post-obduction sedimentary formation consists of thick (100 to 300 m) shallow water carbonate platform deposited on the Sivas ophiolite, referred to as the Tecer Formation (Figure 8a). The contact between the top of the ophiolitic basement and the Tecer Formation defined a paleosurface representing a major unconformity across the Sivas Basin (referred hereafter UM1, Figures 7 and 8a). According to the microfossil content (e.g., Figure 8c), this carbonate platform was deposited between Maastrichtian to Thanetian in a shallow-water, low-energy environment (İnan & İnan, 1990; Kurtman, 1973). This formation is well developed in the Tecer and Gürlevik Mountains, which consist of E-W trending anticlines located on the southern part of the Sivas Basin (Figure 2b). South of the Tecer and Gürlevik Mountains, preservation of

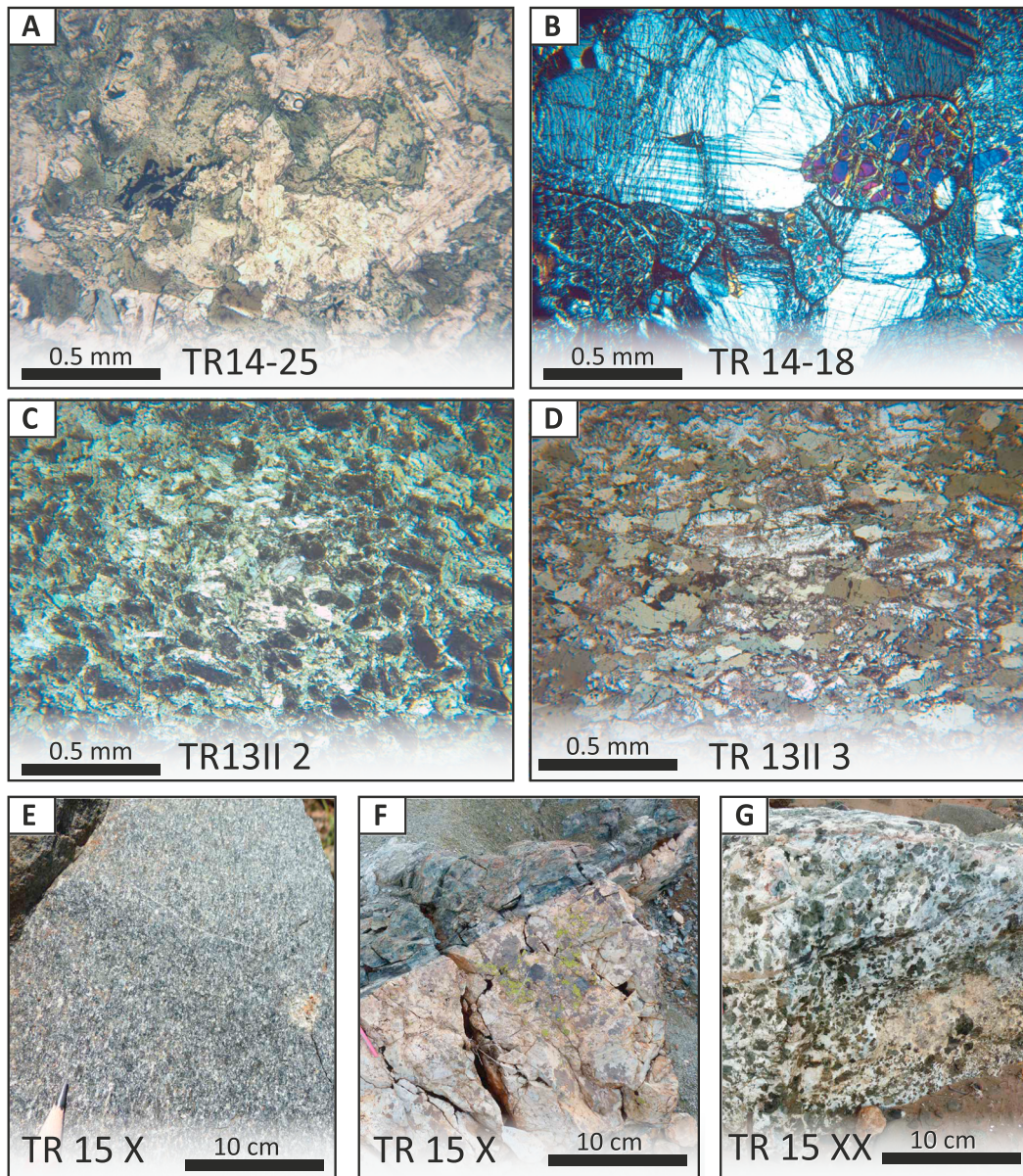


Figure 6. Microscopic and macroscopic photographs of altered mafic rocks observed in the Sivas ophiolite. (a) Amphibolite preserving locally the relics of the coarse-grained magmatic texture, locally the green amphibole may preserve relics of clinopyroxene. (b) Weakly altered troctolite with preserved plagioclase and olivine. (c) Amphibolite. (d) Amphibolite showing locally the shape preferential orientation of euhedral plagioclase and amphibole. (e) Fine-grained metadiorite. (f) Rodingitized dike within the serpentinitized mantle peridotite. (g) Pegmatitic gabbro.

the carbonate platform is highly discontinuous with variable thicknesses, locally only few meters thick. Southward of the Gürlevik Mountain, Maastrichtian sediments, less than 30-m thick, are composed of shallow-water carbonate facies with stromatolites and local rudist patch reefs, directly deposited on top of serpentinite breccias (Figure 8a). Neptunian dykes are observed at the base of the carbonate sequence and within the ophiolitic units. Carbonate sediments filling anastomosed fractures at various angles include centimeter-size clasts of fractured ophiolitic basement (Figure 8a).

Laterally, Upper Cretaceous to Paleocene carbonates with similar fossil content (İnan & İnan, 1990; Kurtman, 1973) are documented toward the South in the Kangal Basin (Baykal, 1945) and toward the East on the Divriği ophiolite (Karacabey, 1972). Toward the north, Late-Cretaceous to Paleocene sediments are represented by an assemblage of deep marine deposits (Legeay, Pichat, et al., 2019). In our study area, the lateral equivalent of the Tecer Formation is the Çerpaçindere Formation (600-m thick) made of siliciclastic-

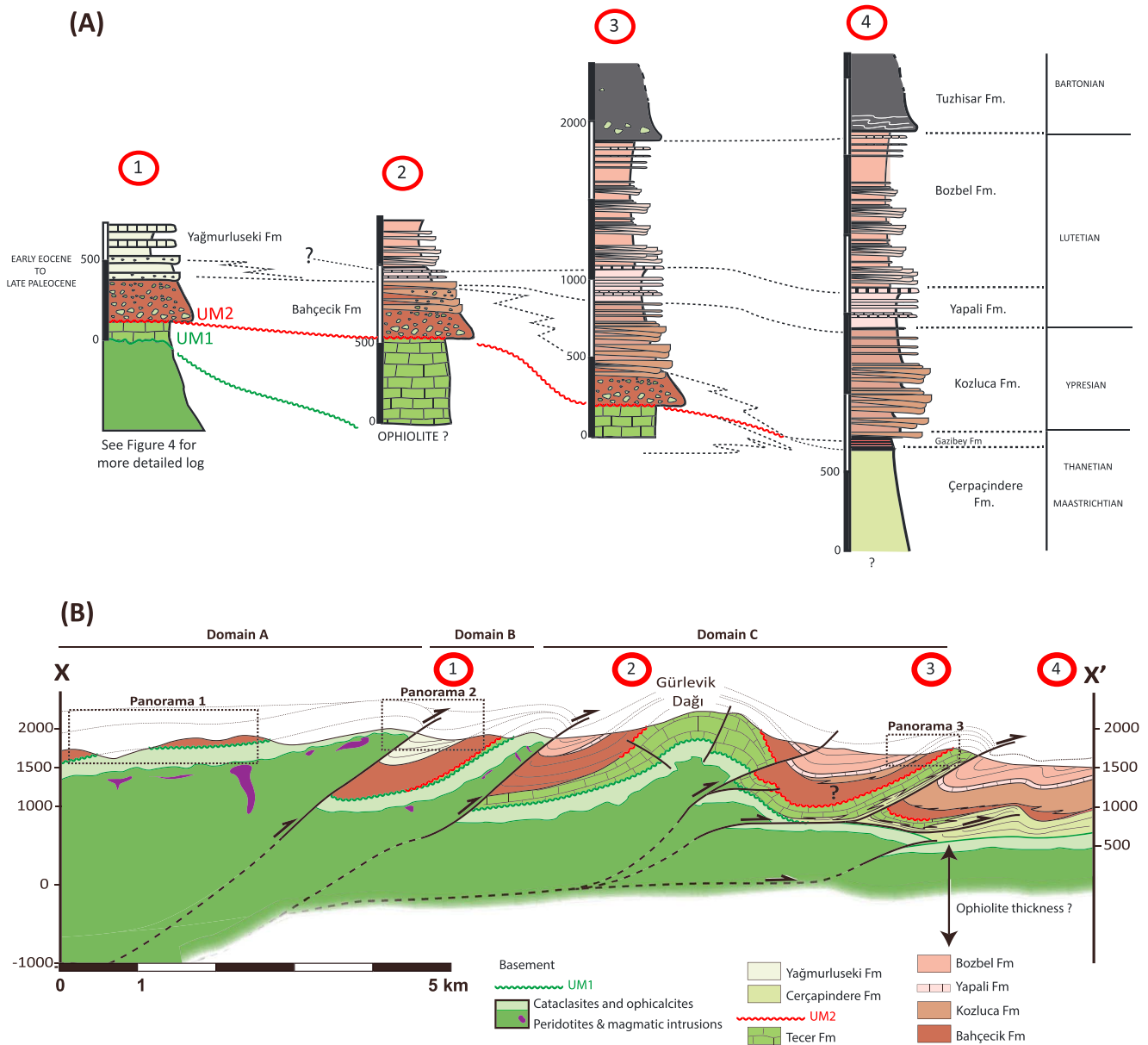


Figure 7. (a) Simplified stratigraphic succession across the southern boundary of the Sivas Basin modified from (modified from Legeay, Pichat, et al., 2019). (b) Cross section across the southern margin of the Sivas Basin (location in Figure 3).

to carbonate-rich turbidities (Aktimur et al., 1990), capped by ~50-m-thick reddish shales (Gazibey Formation; Figures 2b and 7a).

5.2. Late Paleocene to Early Eocene

Around the Gürlevik Mountain, massive conglomerates, breccias, and coarse clastic sediments belonging to the Bahçecik Formation unconformably overlie the Tecer Formation (Figures 8c–8h). An erosional surface between the two formations defines the second regional unconformity UM2 (Figures 7 and 8d). Locally, these massive conglomerates are lying directly over the ophiolite. The conglomerates are generally clast supported, with clast size varying from centimeters to decameters. The clasts consist essentially of serpentinized peridotites and ophicalcites near the base of this formation (Figure 8e), and less frequently of fossiliferous calcarenites near the top with reworked ophiolite related material, and nummulitic limestones (Figure 8h). The thickness of this formation is variable, ranging from 200 m to only 50 m. The irregular

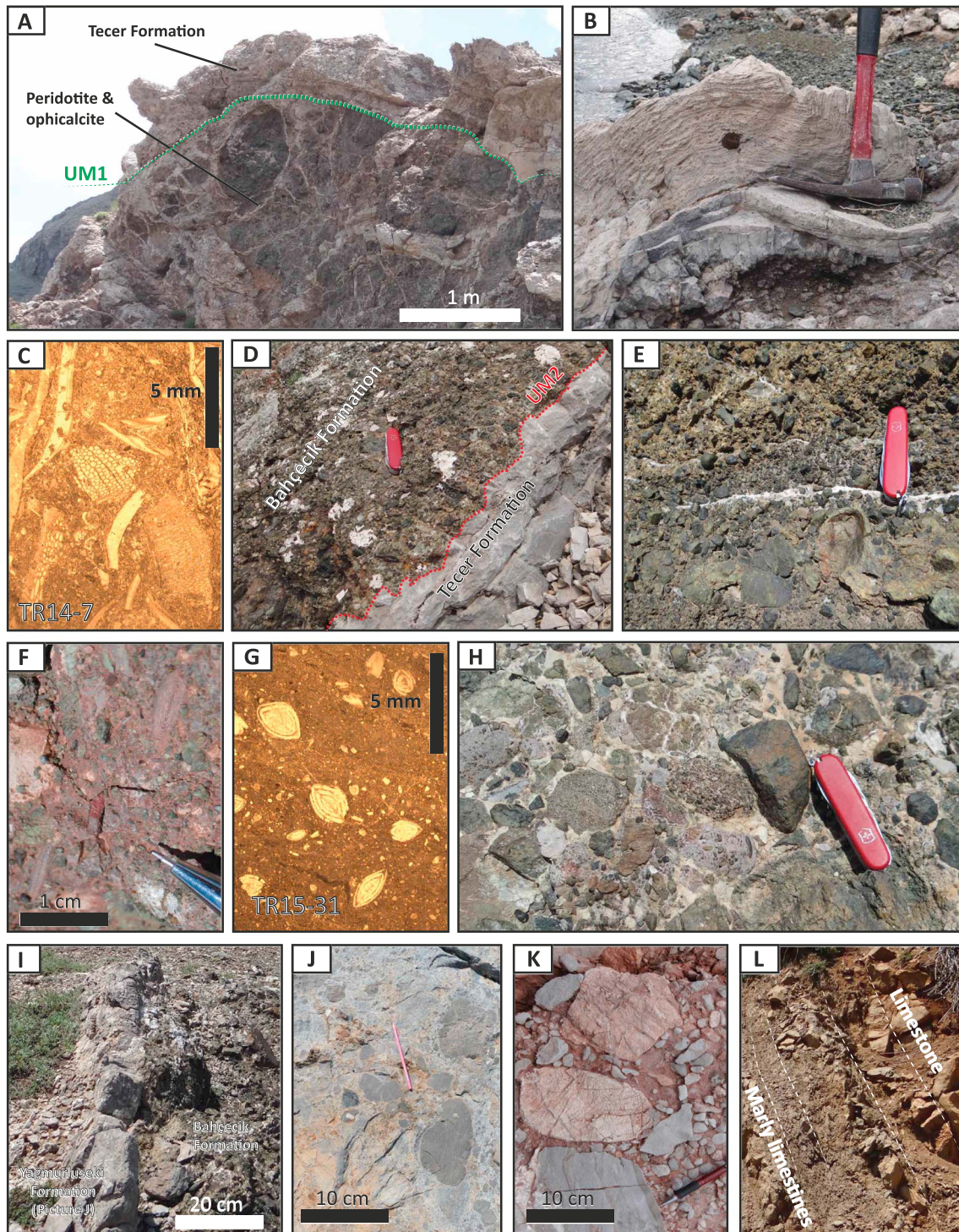


Figure 8. Field pictures from the Maastrichtian to early Eocene sedimentary cover. (a) Depositional surface UM1 delimiting the Tecer formation from the ophiolite, associated with neptunian dykes consisting of carbonate veins ($39^{\circ}33'12.10''N/37^{\circ}31'57.81''E$). (b) Stromatolites from the Tecer Formation emplaced above the ophiolite. (c) Maastrichtian wackestone composed of rudist fragments and benthic foraminifera from the Tecer Formation. (d) Unconformity surface UM2 at the base of Bahçecik Formation above the Tecer Formation (Gürlevik anticline, $39^{\circ}34'28.94''N/37^{\circ}30'9.54''E$). (e) Conglomerate of the Bahçecik formation showing a fining upward sequence. (f) *Nummulites* sp. in conglomerate of the Bahçecik Formation. (g) Wackestone of the Bahçecik Formation, with *Assilina* gr. *Spira* and *Nummulites* gr. *Rotularius* dated as Cuisian (Ypresian). (h) Polygenic conglomerate with calcarenites and mantle-derived clasts of the Bahçecik Formation above the Gürlevik anticline. (i) Contact between a wackestone containing serpentine clasts (picture g) and massive conglomerate made of serpentine clasts at the boundary between Yağmurluseki and Bahçecik Formations (Picture e). (j and k) Conglomerates of the lower Yağmurluseki Formation with Tauride carbonate derived clasts (Ypresian nummulites in matrix), with carbonate supported matrix (j) or red clastic sediments (k). (l) Upper Yağmurluseki Formation with marls and limestones.

spatial distribution and thickness of this sedimentary formation are probably related to a complex paleogeographic framework, with local incised valleys within the Upper Cretaceous to Palaeocene carbonate platform. The age of this formation is bracketed by the underlying Thanetian carbonates (Tecer Formation; Figure 8d) and the overlying Lutetian flysch (Bozbel Formation) around the Gürlevik Mountain (Figure 2b). In addition, microfossils have been found in wackestone calcarenite interstratified with conglomerates south of the Gürlevik Mountain (Figure 8j), directly lying on top of the ophiolite. *Nummulites* gr. *lucasi*, *Nummulites* gr. *rotularius*, and *Assilina* gr. *Spira* were identified, suggesting a late Paleocene to early Eocene age for the deposition of these conglomerates (J. Serra-Kiel, personal communication, 2016; e.g., Figures 8f and 8g).

Toward the north, the massive conglomerates of the Bahçecik Formation pass to the turbidites of the Kozluca Formation, composed of reworked ophiolite related material and volcanoclastic sediments. The facies transition is visible north of the Gürlevik Mountain, near the emergence of north verging thrusts. The Kozluca Formation is interpreted as the distal facies of the Bahçecik Formation because of similar clast composition and fossil content (Kurtman, 1973).

South of the Gürlevik Mountain (Figure 3), mixed clastic and carbonate sediments characterize the Yağmurluseki Formation (50- to 300-m thick). It comprises a lower basal reddish conglomerate reworking clasts derived from the ophiolite and Mesozoic Tauride carbonates (Figures 8j and 8k). It is overlain by red clastic sediments, which are capped by a ten meters thick carbonate (Kavak et al., 1997). This Formation was formerly interpreted as Maastrichtian-Paleocene laterally equivalent to the Tecer Formation (Kavak et al., 1997). However, it can be found on top either of the ophiolitic substratum or of the Late Cretaceous-Paleocene Tecer Formation or of the late Paleocene to early Eocene Bahçecik Formation (e.g., Figures 7b and 8i). Considering our observations in our study area, south of the Gürlevik mountain, we favor a late Paleocene to early Eocene age for the lower part, while the upper carbonate part is possibly an equivalent of the middle Eocene Yapalı Formation.

5.3. Middle to Late Eocene

The Yapalı middle Eocene Formation (Figure 7) consists of fine-grained turbiditic sequences characterized by thin-bedded calcareous interval (150-m thick; Yılmaz et al., 1989) regionally overlying the Kozluca formation (Legeay, Pichat, et al., 2019). It passes upward to thick turbiditic sequences named the Bozbel Formation (up to 700-m thick) which consists of marl rich deposits and fine grained siliciclastic turbiditic sequences with local olistostromes and slumps (Kurtman, 1973). The uppermost part of the Bozbel Formation exhibits a regressive sequence that preceded the deposition of a thick salt level, named the Tuzhisar Formation (see review in Pichat, 2017).

6. Structure of the Southern Margin of the Sivas Basin

The southern margin of the Sivas Basin is characterized by a set of thrust sheets involving the ophiolitic basement, tectonically interleaved and interfolded with the Maastrichtian to Eocene sedimentary cover. Three distinct structural domains (hereafter referred as Domains A, B and C, Figures 9a and 7) have been distinguished in the description below. The distinction between these three domains is based on their distinct stratigraphic record and structural style, and they are delimited by first-order tectonic structures (e.g., Legeay, Ringenbach, et al., 2019). They record key characteristics to depict the Maastrichtian to late Eocene kinematics along the southern Sivas Basin.

Domain A- The domain A formed an elongated E-W trending region dominated by outcrops of the Sivas ophiolite (Figures 9a and 9b). This domain is made of gently folded anticlines with wavelength of 2–3 km and low amplitude (50–200 m) that affect both the ophiolitic basement and the Maastrichtian to early Eocene sedimentary cover. Antiformal structures are separated by north verging thrust faults involving possibly the autochthonous Tauride platform below the obducted Sivas ophiolite. In our study area, this domain is limited to the south by the left-lateral Deliler-Tecer fault (Aktimur et al., 1990; Akyuz et al., 2013). The stratigraphy of the domain A comprises mainly the Tecer and Bahçecik Formations, and eventually the Yağmurluseki Formation which is mostly eroded. To the north, serpentinized peridotites from the domain A are overthrust onto the Yağmurluseki Formation

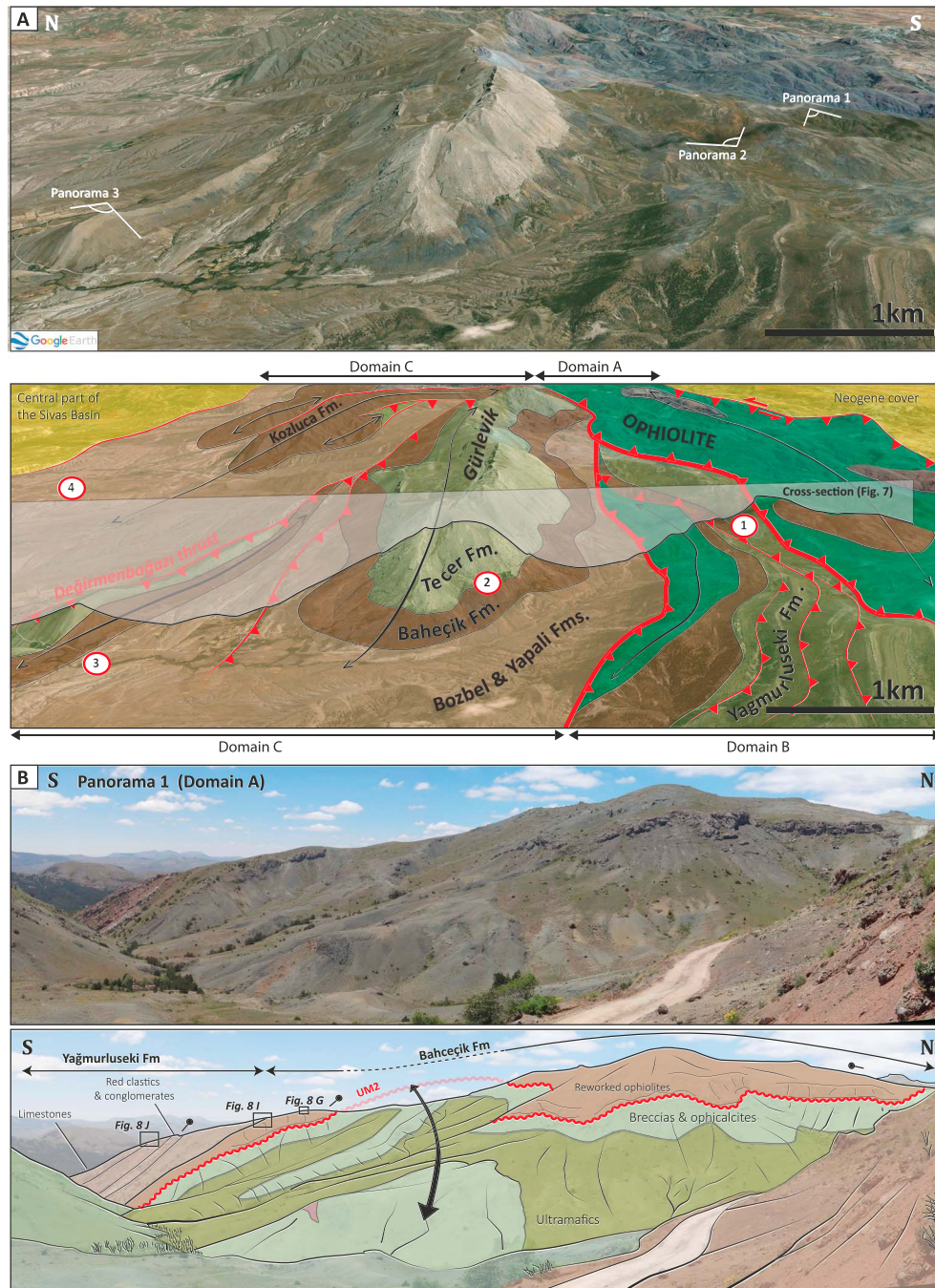


Figure 9. Interpreted panoramas of the study area showing relationships between ophiolite and post-obduction sedimentary cover. Location of the panoramas are presented in Figure 3. (a) Three-dimensional view from Google Earth in the vicinity of the Gürlevik anticline presenting north-verging thrusts separating the distinct tectonic domains A, B, and C. (b) Panorama 1: Anticline folding together the early Eocene Bahçeçik Formation and the ophiolite separated by the UM2.

Domain B– The domain B formed an E-W narrow irregular gutter, wider in the western part of the study area (Figure 2b). To the south, this domain is limited by the north verging thrust of the domain A and to the north by the thrusting of the underlying ophiolitic units over the domain C (Figures 10a and 9a). This frontal structure cuts off both Bozbel and Tuzhisar Formations (Figure 3) and is locally sealed by the passive-roof thrust of the salt domain in the central Sivas Basin (Figure 2b; Kergaravat et al., 2016; Legeay, Pichat, et al., 2019). The thickness of the ophiolitic basement involved in the thrust sheets is about 500 m. Considering the maximum thickness of the ophiolitic sequence outcropping today (>1,000 m), the decollement

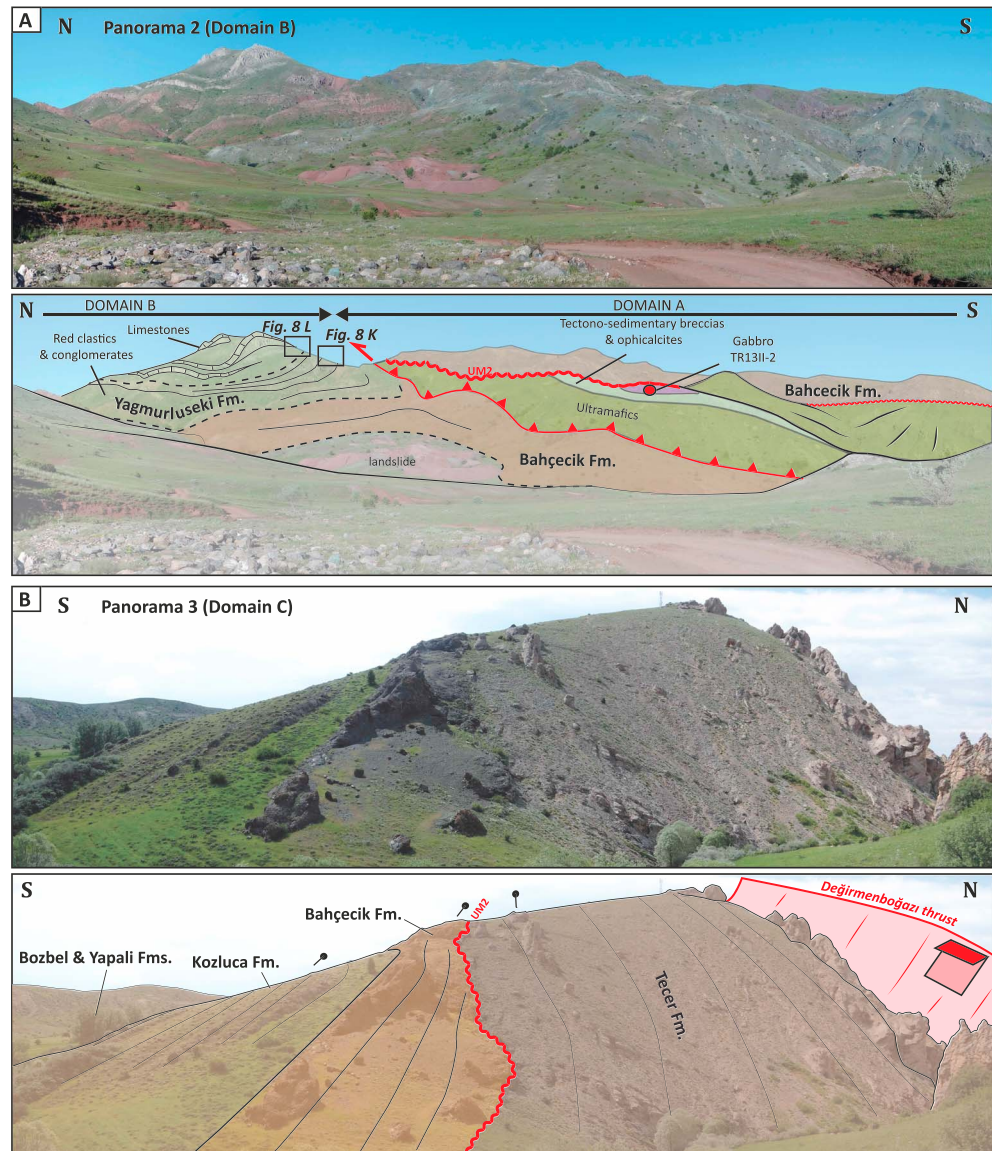


Figure 10. Interpreted panoramas exhibiting the general structure of the study area. (a) Panorama 2: South of the Gürlevik anticline, imbricated ophiolitic thrust sheets and Eocene cover. (b) Panorama 3: Along the road toward the Village of Değirmenboğazi, the preserved Late Cretaceous to Eocene sedimentary succession is made of Late Cretaceous-Paleocene shallow-marine carbonate platform (Tecer Fm), early Eocene conglomerates (Bahçecik Formation), and late Eocene turbidites (Bozbel Formation). The UM2 unconformity separating the Tecer and Bahçecik Formations can be well recognized. Panorama showing the ophiolitic basement thrust above the domain B, directly on top of Eocene clastic sediments and carbonates.

level may be located within the obducted ophiolite itself. Along the western edge of the domain, several shallower thrusts, affecting the Paleogene sedimentary cover, show a short spacing (300–500 m), passing to the east to a well exposed syncline (Figure 10a). The sedimentary succession composing the syncline comprises (1) the ophiolitic basement delimited at its upper limit by the major unconformity (UM1) likely associated with significant erosion, (2) a few meters of the Maastrichtian to Paleocene carbonate platform (Tecer Formation) capped at the top by the UM2 unconformity, (3) conglomerates made of ophiolitic clasts (Bahçecik Formation), and (4) conglomerates with carbonate clasts, followed by red clastic sediments and shallow water carbonate platforms (Yağmurluseki Formation). The Yağmurluseki Formation is locally interpreted as a syntectonic infill of the growing

syncline (Figure 10a) highlighted by thickness variations, growth strata along the thrust, and a small wedging toward the north.

Domain C- The domain C is limited to the south by a north verging thrust involving locally the ophiolite (Figures 10b and 9b) and to the north by the south verging passive-roof thrust (Figures 2 and 3). Considering the wavelength and amplitude of the Gürlevik anticline made of the Tecer Formation, the implication of the underlying ophiolitic basement is suspected (see cross section Figure 7b). North of the Gürlevik anticline, this domain comprises E-W elongated folds with long wavelength (2–3 km) and large amplitude (200–500 m). These anticlines are locally faulted as exemplified by the Değirmenboğazi thrust, which is well exposed in the landscape (Figure 2b). Decollements may root in Maastrichtian-Paleocene turbidites as described further east (Aktimur et al., 1990). The domain C records the most complete Maastrichtian to Eocene stratigraphy, with the exception of the Yağmurluseki Formation. The section on the hanging wall of the Değirmenboğazi thrust (Figures 7b and 10b) highlights the general stratigraphy of this domain comprising the strong erosional unconformity UM2 on the top of Tecer Formation, the progressive transition from conglomerates (Bahçecik Formation) to turbidites made of volcanoclastic/ophiolitic materials (Kozluca Formation). Eventually, the stratigraphic record continues until the Tuzhisar Formation, which is preserved below the thrust delimiting the domain C, and within tight synclines to the west of the Tecer Anticline (Figure 2b).

7. Whole Rock Geochemistry of Mafic Intrusive Rocks

Petrological observations reveal that all the samples, for which major and trace element data were obtained, underwent hydration and metamorphism under greenschist to amphibolite facies conditions.

The analyzed metamicrogabbro to metamicrodiorite from the Sivas ophiolite show SiO₂ contents ranging from 47 to 55 wt% (Table 1 and Figure 11). Despite the strong alteration observed at thin section scale, loss of ignition (LOI) ranges between 1.4 and 3.8 wt%. Our rock classification and geotectonic discrimination diagrams are based on high field strength elements (HFSE) and immobile trace elements. The Nb/Y-Zr/TiO₂*0.0001 diagram (after Winchester & Floyd, 1977; Figure 11a) is used for rock classification, and two geochemical diagrams (TiO₂-V, Shervais, 1982, and Zr-Zr/Y, Pearce & Norry, 1979; Pearce, 2003; Figures 11b and 11c) are shown to investigate the geodynamic context in which these mafic intrusions were emplaced. They are completed by Th-Co (after Hastie et al., 2007) and Th/Yb-Nb/Yb (Dilek & Furnes, 2009; Pearce, 2008) diagrams provided in supporting information Text S2. On the TiO₂-V diagram (after Pearce, 2003), all analyzed rocks can be divided in two groups, namely, groups 1 and 2, showing Ti/V ratio between 10 and 20 and Ti/V close to 20, respectively. Such Ti/V ratio especially for the group 1 is typical for forearc basalts (Pearce, 2003; Dilek et al., 2007). Similar geochemical fingerprint can be derived from the Zr-Zr/Y diagram, groups 1 and 2 being on the fields of the boninites and of the island arc tholeiites, respectively.

On a chondrite-normalized rare earth elements (REE) diagram, the two groups can be equally well identified (Figure 11d). Group 1 shows a relative depletion of light REE (LREE) over heavy REE (HREE), associated locally with U-shaped LREE patterns. Group 2 is characterized by an enrichment in LREE relative to HREE, the latter showing a flat pattern.

A normal mid-ocean ridge basalt (NMORB) normalized multielement diagram is shown in Figure 11e. The mafic rocks display a similar pattern, although the two main groups previously identified can also be distinguished here. Both groups are characterized by strong enrichment in large ion lithophile elements (LILE) such as K, Sr, Rb, and Ba. In general, group 1 shows stronger positive LILE anomalies than group 2. In contrast, high field strength elements (HFSE) such as Nb and Zr present negative anomalies, again more important for group 1.

Diagrams of Ni, Cr₂O₃, Zr, TiO₂ using the bulk-rock Mg# as differentiation index are shown in supporting information Text S3 documenting possible distinct degrees of magmatic differentiation, group 1 being more primitive than group 2.

8. Zircon U-Pb Dating of the Mafic Intrusive Rocks

Two samples for the mafic intrusive rocks from the Sivas ophiolite were collected for laser ablation inductively coupled plasma mass spectrometry (LA-ICP-MS) U-Pb zircon dating. The two dated samples (TR 13

Table 1
Major and Trace Element Composition of the Magmatic Rocks Sampled in the Sivas Ophiolite

Analyte	Unit	GROUP 1								GROUP 2				
		TR 13 II-2	TR 13 II-3	TR 13 II-6	TR 13 II-7	TR 14-24	TR 14-32	TR 14-33	TR 14-42	TR 14-25B	TR 14-26	TR 14-28	TR 14-29	TR 14-30
SiO ₂	%	51.43	50.35	48.15	49.71	46.46	50.37	47.13	48.24	52.82	49.23	50.47	52.09	54.27
Al ₂ O ₃	%	15.51	15.58	9.37	14.95	13.61	15.91	13.88	15.64	14.62	15.6	15.95	15.31	15.48
Fe ₂ O ₃	%	7.83	8.09	10.71	8.69	7.86	9.28	9.13	7.62	8.81	9.79	10.86	10.87	11.83
MgO	%	8.24	8.5	13.37	8.62	8.58	7.75	10.05	8.49	8.12	8.3	7.42	6.44	3.9
CaO	%	11.01	11.35	14.16	11.46	18.46	8.36	14.38	13.73	10.21	8.79	5.66	6.5	4.58
Na ₂ O	%	3.05	2.79	0.34	2.59	0.31	2.97	1.03	1.26	2.49	2.82	3.7	4	6.12
K ₂ O	%	0.31	0.43	0.04	0.35	0.14	1.64	0.27	1.42	0.31	1.15	1.62	1.2	0.56
TiO ₂	%	0.47	0.48	0.58	0.43	0.4	0.7	0.47	0.57	0.69	1	1.15	1.13	1.3
P ₂ O ₅	%	0.02	0.03	0.02	0.01	0.03	0.04	0.03	0.03	0.09	0.08	0.08	0.08	0.1
MnO	%	0.12	0.13	0.16	0.15	0.12	0.17	0.15	0.15	0.16	0.16	0.18	0.18	0.17
Cr ₂ O ₃	%	0.042	0.045	0.013	0.041	0.057	0.014	0.053	0.017	0.05	0.019	0.006	0.007	<0.002
Ba	PPM	145	115	<5	65	15	86	22	171	77	54	95	97	40
Ni	PPM	107	106	223	95	131	69	136	64	94	73	36	33	<20
Sr	PPM	770	719	16	139	76	214	136	105	108	199	614	382	231
Zr	PPM	21	18	20	17	22	37	16	33	57	58	65	65	77
Y	PPM	11	12	14	12	10	18	13	13	21	22	25	25	30
Sc	PPM	37	39	41	38	35	35	43	37	37	37	37	37	33
LOI	%	1.7	1.9	2.8	2.8	3.8	2.6	3.2	2.6	1.4	2.8	2.6	1.9	1.5
Sum	%	99.82	99.81	99.74	99.81	99.83	99.84	99.8	99.83	99.84	99.81	99.83	99.84	99.86
Ba	PPM	161	125	6	77	19	87	22	180	87	59	98	111	45
Be	PPM	<1	<1	<1	<1	<1	<1	<1	<1	<1	<1	<1	<1	<1
Co	PPM	34.7	34.9	49	35.6	32.4	33.4	42.4	34.4	31	38.2	37.8	34.9	31.7
Cs	PPM	4.9	4.1	<0.1	<0.1	<0.1	0.4	0.5	<0.1	<0.1	2.1	0.3	0.2	<0.1
Ga	PPM	12.7	12	9.3	10.7	10.8	13.7	10.7	12	15	13.3	14.6	14.2	16.5
Hf	PPM	0.8	0.7	0.7	0.8	0.7	1.2	0.6	0.8	1.8	1.7	2	2	2.4
Nb	PPM	0.4	0.3	0.3	0.8	1.1	0.6	0.5	0.5	1.9	1.1	1	1.4	1.4
Rb	PPM	4.9	4.6	0.3	3.8	1.1	17.2	3	7.2	4.7	19.2	18.6	12.8	4
Sn	PPM	1	<1	<1	<1	<1	<1	<1	<1	<1	<1	<1	<1	<1
Sr	PPM	837.6	767.4	18.7	153.8	80.9	225.7	142.3	107.6	119.6	222.2	675.3	415.4	241.8
Ta	PPM	<0.1	<0.1	<0.1	0.4	0.1	<0.1	<0.1	<0.1	0.1	0.1	<0.1	0.1	0.6
Th	PPM	<0.2	<0.2	<0.2	0.5	0.2	<0.2	<0.2	0.2	1.7	0.4	0.3	0.4	0.6
U	PPM	<0.1	<0.1	<0.1	<0.1	<0.1	<0.1	<0.1	<0.1	0.1	0.1	<0.1	<0.1	0.2
V	PPM	258	259	262	252	214	294	284	218	183	279	304	311	428
W	PPM	<0.5	<0.5	0.6	3.9	1	<0.5	<0.5	<0.5	7.6	7	3.7	3	3
Zr	PPM	20	18	19.8	24.2	21.6	36.4	14.3	31.9	64.5	58.1	64.8	70.6	76.3
Y	PPM	12.1	12.3	13.4	12.2	10.4	17.6	12.2	12.2	20.9	21	24.6	25.1	30.4
La	PPM	1.2	2.1	1.3	7.6	2.5	1.8	1	1.6	10.3	5.2	3.8	7.4	9
Ce	PPM	3	4.4	3.7	18.2	4.5	4.2	2.4	4.5	23.6	12.9	10.6	17.4	20.8
Pr	PPM	0.39	0.58	0.54	2.2	0.49	0.66	0.35	0.6	2.88	1.7	1.6	2.37	2.79
Nd	PPM	2.6	3.2	2.9	8.5	2.4	4	2.2	3.3	12.6	8.3	8.6	11.2	13.1
Sm	PPM	0.73	1.04	1.2	1.94	0.91	1.37	0.94	1.18	3.03	2.54	2.43	3.17	3.3
Eu	PPM	0.34	0.36	0.44	0.55	0.35	0.54	0.34	0.49	1.01	0.93	0.96	0.97	1.22
Gd	PPM	1.4	1.46	1.82	1.7	1.31	2.16	1.49	1.71	3.45	3.24	3.7	3.95	4.4
Tb	PPM	0.28	0.29	0.35	0.33	0.26	0.4	0.29	0.32	0.58	0.58	0.67	0.72	0.81
Dy	PPM	1.97	2.06	2.35	2.13	1.61	2.73	2.11	2.15	3.68	3.84	4.24	4.44	5.21
Ho	PPM	0.44	0.5	0.53	0.52	0.45	0.65	0.49	0.48	0.84	0.9	0.94	1.02	1.25
Er	PPM	1.4	1.39	1.64	1.33	1.27	1.96	1.4	1.51	2.45	2.5	2.83	2.76	3.51
Tm	PPM	0.21	0.2	0.23	0.21	0.18	0.28	0.19	0.18	0.35	0.37	0.4	0.42	0.52
Yb	PPM	1.21	1.4	1.5	1.48	1.34	1.97	1.39	1.25	2.42	2.47	2.77	2.66	3.32
Lu	PPM	0.2	0.21	0.26	0.24	0.2	0.27	0.2	0.18	0.37	0.39	0.4	0.45	0.53
Ti/V		10.92	11.11	13.27	10.23	11.21	14.27	9.92	15.68	22.60	21.49	22.68	21.78	18.21
Mg Number		0.68	0.68	0.71	0.66	0.68	0.62	0.69	0.69	0.65	0.63	0.58	0.54	0.40

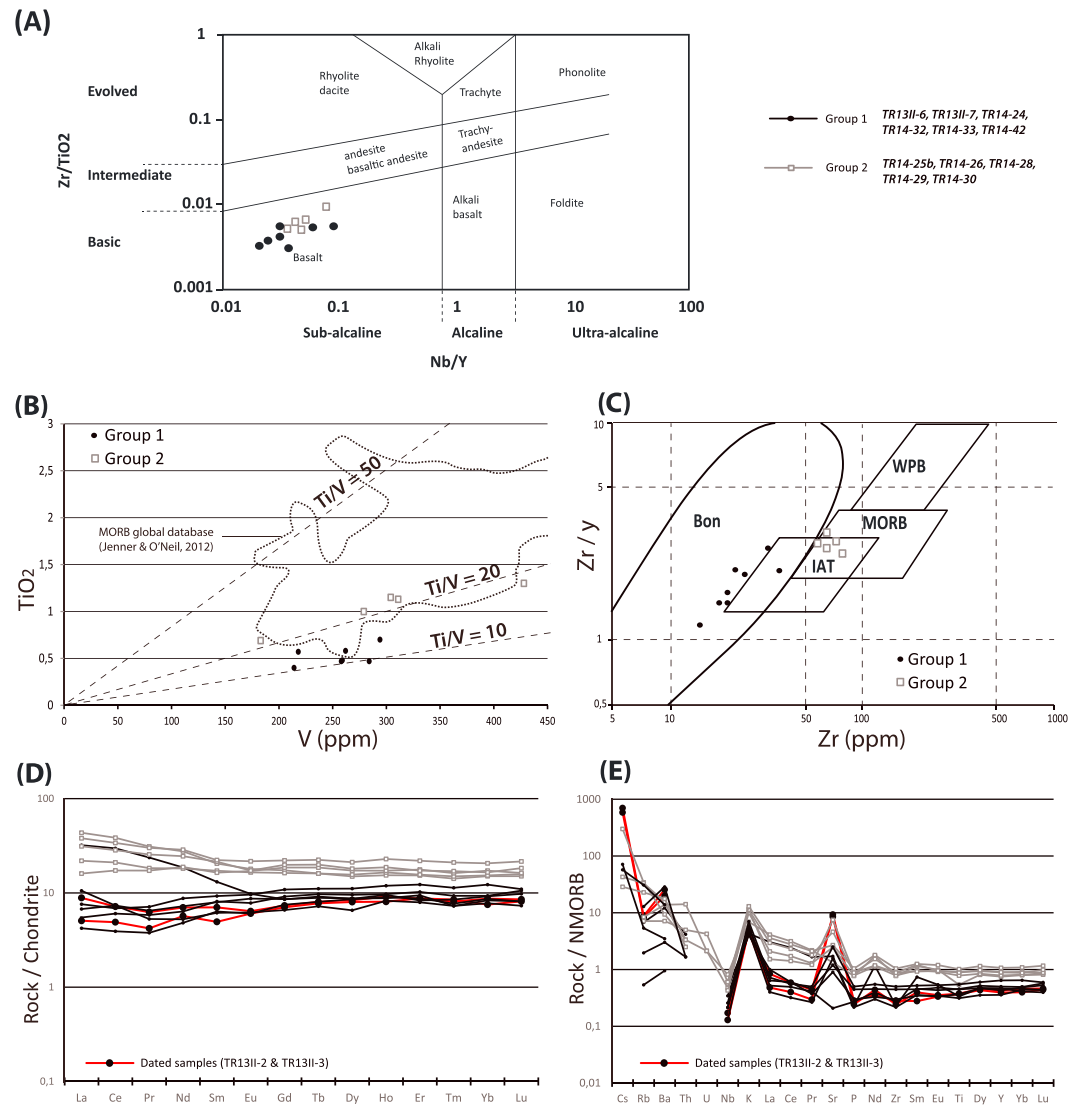


Figure 11. Discriminant geochemical diagrams of the magmatic rocks of the Sivas ophiolite. (a) Nb/Y- Zr/TiO₂*0.0001 discrimination diagram (after Winchester & Floyd, 1977). (b) TiO₂ versus V (Shervais, 1982) and (c) Zr-Zr/Y (after Pearce & Norry, 1979; Pearce, 2003). (d) Rare earth element diagram of the studied samples normalized to chondrolite (Sun & McDonough, 1989). (e) Trace element diagram normalized to NMORB (Sun & McDonough, 1989). MORB = mid-oceanic ridge basalts; IAT = island arc basalts; WPB = within plate basalts; Bon = boninites

II-2 and TR 13 II-3; see Figure 2 for sample location) were collected from a few meters thick mafic dikes intruding the serpentinized peridotite massif, south of the Gürlevik anticline. Analytical method is presented in supporting information Text S1 and radiogenic ratio in supporting information Text S4. For the Concordia age calculation discordant ages were discarded based on a concordancy level of 95%–105%.

8.1. Sample Description

Sample TR 13 II-2 is a fine-grained amphibolite containing plagioclase + green amphibole ± epidote (Figure 6c). The initial magmatic texture is locally preserved as demonstrated by the presence of euhedral to subhedral plagioclase (<1 mm in size). The magmatic plagioclase is mostly replaced by a fine-grained aggregate of secondary albite + chlorite + sericite. This sample was likely a microdiorite/gabbro that subsequently underwent significant hydrothermal metamorphism under greenschist facies conditions.

The sample TR 13 II-3 was taken a few meters from the previous sample and consists of a medium-grained metagabbro/diorite that significantly recrystallized during hydrothermal metamorphism (Figure 6d). This sample is made of plagioclase and green amphibole. It is characterized by the

development of a weak fabric characterized by the shape-preferred orientation of both plagioclase and amphibole. Magmatic euhedral to subhedral plagioclase (~1–5 mm in size) is observed, although often replaced by fine-grained aggregates of albite + chlorite + sericite. Green amphibole is abundant and includes in places clinopyroxenes.

8.2. Zircon U-Pb Dating Ages

8.2.1. Sample TR 13 II-2

Six analyses were performed on seven zircons. Based on the cathodoluminescence (CL) images, the zircon grains show rounded to irregular outlines with a size up to 120 μm in length and 50 μm in width (Figure 12). All the zircon grains are uniformly dark in CL images. The analyses on five zircons are concordant to subconcordant defining a Concordia age of 72.7 ± 0.5 Ma [mean square of weighted deviates (MSWD) = 0.26; Figure 12].

8.2.2. Sample TR 13 II-3

Fourteen analyses were performed on 22 zircons. Zircon grains imaged by CL are up to 200 μm in length and 80 μm in width. In general, zircon grains show irregular subrounded to rounded crystal shapes displaying homogenous textures. Locally, few elongated zircon grains with oscillatory zoning are observed (Figure 12). The analyses define a main population and yield a Concordia age of 91.49 ± 0.8 Ma (MSWD = 0.41; Figure 12). In addition, a younger population of five zircons define a Concordia age of 87.8 ± 1.5 Ma.

9. Discussion

9.1. Pre-Obduction Evolution of the Sivas Ophiolite

9.1.1. Lithostratigraphic Association and Architecture of the Sivas Ophiolite

The Sivas ophiolitic sequence is characterized by highly serpentized peridotites with sparse magmatic intrusions (e.g., microgabbro and microdiorite) showing significant metamorphic recrystallizations in greenschist to amphibolite facies conditions. The top of the serpentized mantle is consistently capped by a zone of brittle deformation localized in the first 50 to 100 m and exhibiting an increasing deformation gradient toward the top. The top of the ophiolitic sequence is likely incomplete as shown by absence of extrusive magmatism (i.e., pillow basalt) or/and pre-obduction sediment deposition at the seafloor, except from rare occurrence of cherts, serpentinite breccias, and arenites. This lack of pelagic sediments and extrusive magmatism may be the result of local subaerial erosion during final stages of obduction before the deposition of post-obduction Maastrichtian sediments. Notably, the observed brittle deformation at the top of the mantle is absent in the overlying post-obduction sediments suggesting a pre-obduction, that is, oceanic, origin. In addition, the observed metamorphic overprint of the mafic rocks within the serpentized mantle is not documented in the overlying Late Cretaceous to Paleogene sedimentary successions. Therefore, this evolution is likely related to the emplacement within the mantle of mafic intrusions that underwent secondary pervasive hydrothermal metamorphism. The brittle deformation consistently localized at the top of serpentized peridotites is interpreted to result from the activity of an extensional detachment fault that exhume these ultramafic to mafic suites to the seafloor (Cannat et al., 2006; Péron-Pinvidic & Manatschal, 2009; Whitmarsh et al., 2001). The activity of this extensional detachment fault led to an intense cataclastic deformation of the mantle, together with significant hydrothermal circulation near the seafloor likely responsible for the observed opicalcites (Figure 13).

Our observations suggest that the Sivas ophiolite samples a “coherent” ophiolitic unit, preserving initial pre-obduction lithological contacts. Notably, the lithostratigraphic association of the Sivas ophiolite differs from the “classical” Penrose type sequence and also from ophiolitic sequences described in the IAEZ and ITSZ (Parlak et al., 2006; Parlak, Çolakoğlu, et al., 2013; Robertson, 2002; Robertson, 2004; Robertson, Parlak, Ustaömer, et al., 2013; Sarıfakıoğlu et al., 2009; Topuz et al., 2013; Uysal et al., 2015; Yalınız et al., 2000; Yalınız & Göncüoğlu, 1998). All together similar observations are commonly described in present-day slow- and ultraslow-spreading ridges often in relation with oceanic core complex (e.g., Cannat et al., 1992; Ildefonse et al., 2007).

Lithostratigraphic association and field relationships described here have also been observed in several others ophiolites of Turkey (Morris et al., 2017) and south Tibet by Maffione, van Hinsbergen, et al. (2015). These authors proposed that such dismembered ophiolites may result from a mechanism defined

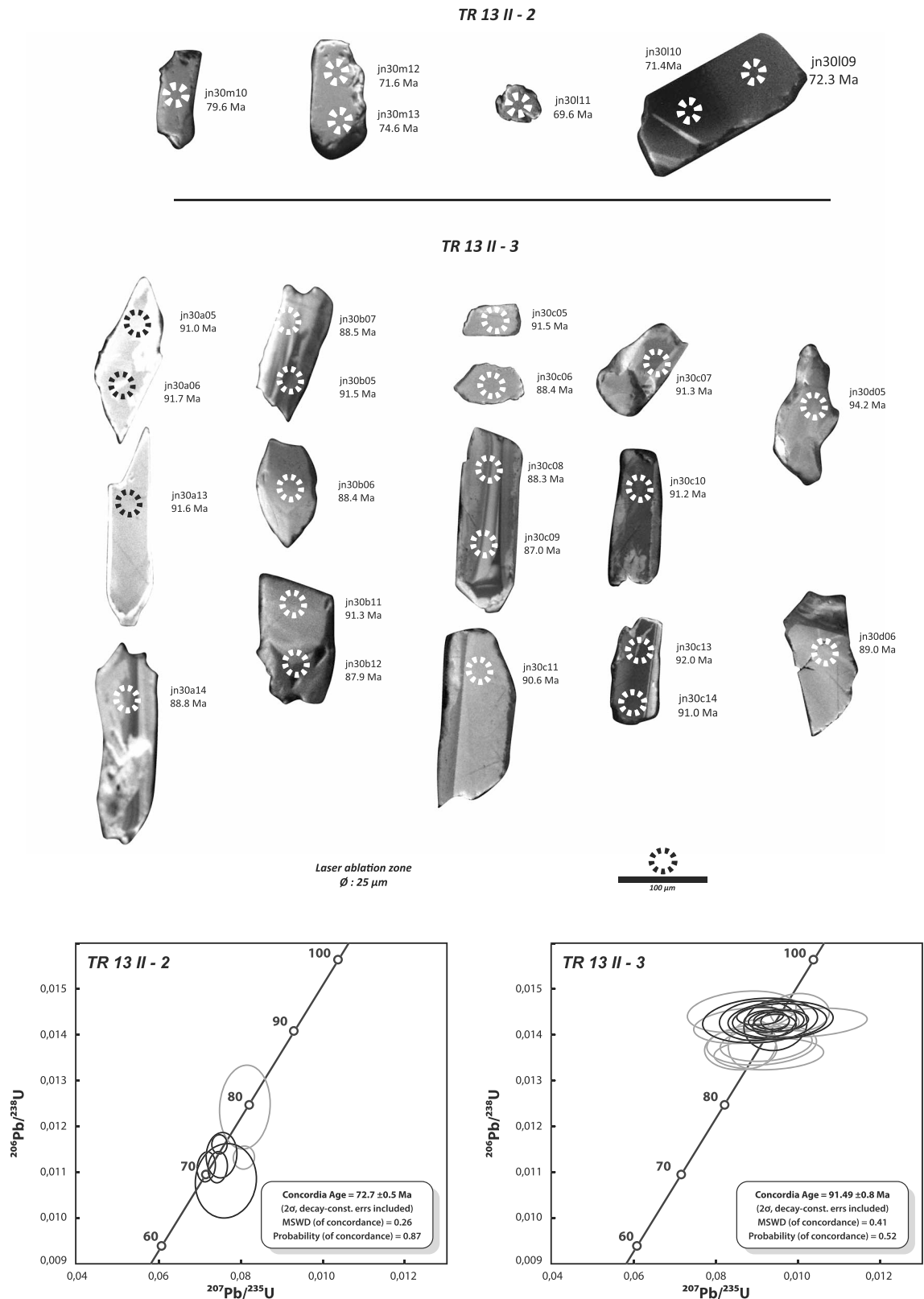


Figure 12. Cathodoluminescence images of zircons from the dated magmatic rocks with dated shot points, and associated Concordia diagrams for the dated samples. The location of the dated samples is shown in Figure 2. Concordia diagrams were calculated using Isoplot/Ex 3.75 (Ludwig, 2012); grey ellipses were not used for age calculation.

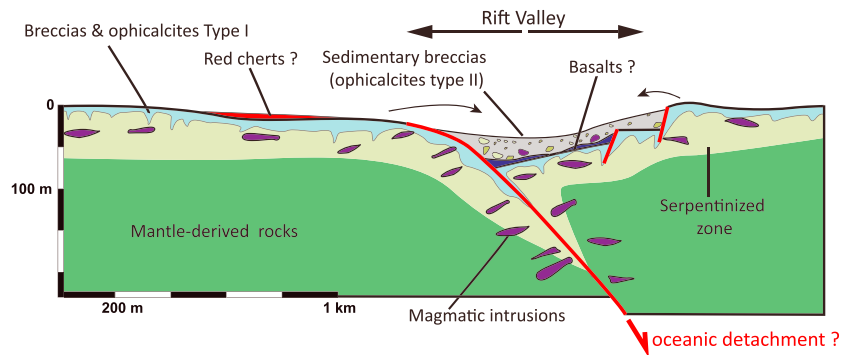


Figure 13. Reconstruction of the pre-obduction setting of the Sivas ophiolite (modified from Maffione, Thieulot, et al., 2015; Maffione, van Hinsbergen, et al., 2015), replacing possible location of the observed lithologies.

as “forearc hyperextension,” whereby stretching of the forearc region during the first few million years of subduction initiation lead to lithosphere (the future ophiolite) thinning and disruption.

9.1.2. Ages and Nature of Magmatic Intrusions

U-Pb analyses of magmatic zircons from the two sampled intrusions in the Sivas ophiolite gives 91.49 ± 0.8 Ma and 72.7 ± 0.5 Ma, respectively (Figure 12). These ages are interpreted as the time of crystallization of the intrusive rocks in the serpentinized mantle. Both age intervals were widely documented in the Turkish ophiolites (see review of van Hinsbergen et al., 2016). The oldest age from the Sivas ophiolite of 91.49 ± 0.8 Ma is in general agreement with U-Pb zircon dating on gabbro cumulates and contemporaneous with ^{40}Ar - ^{39}Ar data from the metamorphic sole at the base of the Tauride ophiolites (e.g., Parlak et al., 2006). Notably, the obtained ages are coherent with the results of Parlak, Çolakoğlu, et al. (2013) in the Divriği ophiolite, southeast of the Sivas ophiolite. In contrast, the younger age of 72.7 ± 0.5 Ma is a few million years older than the deposition of the shallow-marine Maastrichtian-Paleocene carbonate platform over the obducted ophiolite. Similar younger ages of mafic dike intrusions have been already observed in other ophiolites of Turkey (Lycian, Mersin, and Alihoca ophiolites; Dilek & Furnes, 2014; Dilek et al., 1999; Parlak et al., 2006; Parlak, Karaoğlu, et al., 2013).

Recent studies (Maffione, Thieulot, et al., 2015; van Hinsbergen et al., 2015) interpreted these dikes as late-stage magmatic events cross cutting the metamorphic sole, related to intraoceanic subduction, just before obduction. Such relationships confirm the complex and polyphase magmatic evolution associated with intraoceanic subduction and eventual ophiolite obduction.

The geochemical data obtained in this study from the intrusions in the Sivas ophiolite do not always allow for a straightforward interpretation, as the possibility of postcrystallisation uptake of the LILE and even LREE (given their quite low contents in the igneous protoliths) cannot be entirely ruled out. Still, a general enrichment in LILE and LREE relative to HFSE is a feature observed in the studied rocks. Such enrichment was interpreted as a general marker for the suprasubduction zone setting (Metcalf & Shervais, 2008; Saunders et al., 1980; Shervais, 1982; Wood, 1980). The possible influence of a subduction zone is confirmed by the geotectonic discriminant diagrams (Figure 11) highlighting geochemical fingerprints of forearc basalts to island arc tholeiites and even boninites. In the REE distribution, rocks from group 1 show nonpronounced U-shaped LREE patterns, while rocks from group 2 display a general enrichment in LREE. Such enrichment has been explained as the result of the partial melting of a metasomatized mantle enriched in incompatible elements during intraoceanic subduction and related to the percolation of a slab-derived fluid. All the diagrams from the whole rock geochemistry data point to a suprasubduction affinity for the sampled mafic intrusive rocks of the Sivas ophiolite.

Finally, our geochronological and geochemical results across the Sivas ophiolite are coherent with the adjacent Tauride ophiolites (e.g., Divriği ophiolite, located 30 km to the south, Parlak et al., 2006; Parlak, Karaoğlu, et al., 2013) and also more generally with Anatolian ophiolites characterized by similar ages and showing supra subduction zone geochemical signature (e.g., Dilek et al., 1999; Parlak, Karaoğlu, et al., 2013).

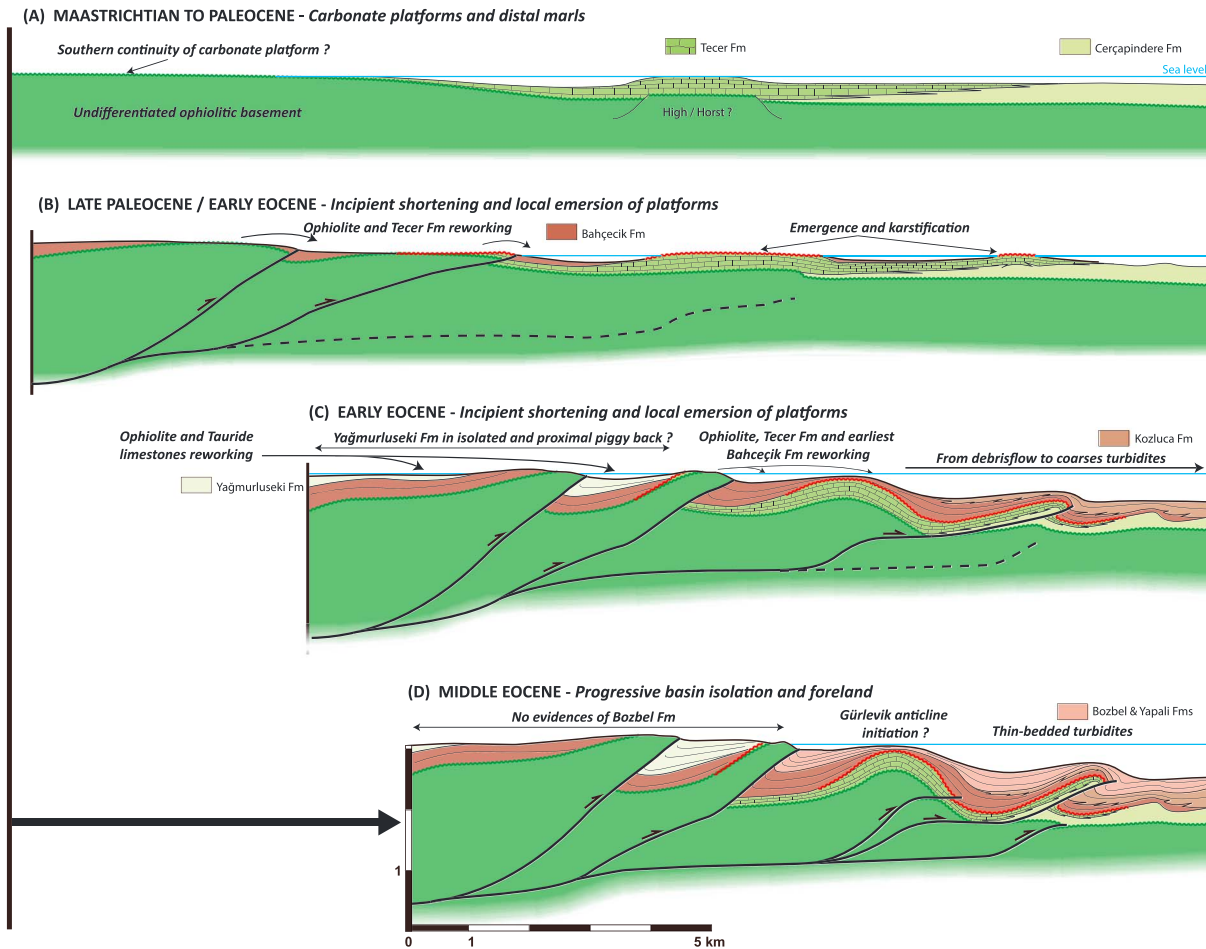


Figure 14. Tectonosedimentary schematic evolution of the Southern Sivas Basin from Maastrichtian to middle Eocene time. These sections are integrated in their regional setting in Figure 15.

9.2. Post-Obduction Evolution of the Southern Sivas Basin

The Sivas ophiolite was obducted over the northern edge of the Tauride margin (see Poisson et al., 2016) during the Late Cretaceous. From Late Cretaceous to Eocene, it recorded a complex post-obduction tectonosedimentary evolution resumed in the Figure 14.

During Maastrichtian-Palaeocene time (Figure 14a), the shallow water carbonate platform of the Tecer Formation developed directly over the ophiolite along the shelf break of the Southern Sivas Basin. Thick carbonate reefs are exposed in the Gürlevik and Tecer anticlines passing laterally farther north to slope and turbiditic sequences of the Çerpaçindere Formation deposited in a deep marine basin. No extensional deformation was observed during the Maastrichtian to Paleocene along the Southern Sivas Basin, but it is documented in adjacent area such as in the Ulukışla Basin (Gürer et al., 2016).

The uppermost Palaeocene to early Eocene period (Figure 14b) recorded evidence for tectonic inversion with incipient contraction along the southern basin edge. Emergence of the ophiolite and Maastrichtian-Palaeocene carbonate platforms is marked by local erosion and karstification. These carbonate reefs and platforms have been dismembered and reworked as olistoliths within ophiolitic conglomerates feeding progressively the basin (Bahçeçik Fm), deposited laterally over either the ophiolite or the Tecer Formation.

During early Eocene time (Figure 14c) the shortening resulted in in-sequence deformation and thrust sheet emergences. In the southernmost area, the conglomerates of Yağmurluseki Formation are deposited in piggy-back basins that have been partially isolated from the open-marine condition, farther to the north. The clast composition of these conglomerates is composed of the dismembered ophiolite and of the

Mesozoic Tauride carbonates. Such conglomerates suggest the occurrence of relief and erosion, south of the Sivas Basin in the Eastern Tauride. It may correspond to the Afyon accretion zone, which was exhumed during Paleocene to early Eocene toward the West (Gürer, Plunder, et al., 2018; Pourteau et al., 2013). Farther north, prograding clastic discharges essentially derived from the ophiolite are deposited in the Sivas Basin over the Maastrichtian-Paleocene carbonate platform. In the distal part, the Kozluca Formation interfered with the Bahçecik Formation. Artan and Sestini (1971) reported that turbidites from the Kozluca Formation are composed of both ophiolitic and volcanoclastic materials with southwest oriented paleocurrents.

At middle Eocene time (Figure 14d), a regional transgression has been reported in the Eastern Tauride. In the Sivas Basin, this transgression is associated with the deposition of carbonates (Yapalı Formation) in piggy-back basins at the top of the Yağmurluseki Formation. The turbiditic sequences of the Bozbel Formation have been later deposited toward the north associated with relatively small synorogenic structures, frontward of the Gürlevik anticline (Legeay, 2017; Legeay, Pichat, et al., 2019). During late Eocene time, a thick and widespread evaporite sequence was deposited in the Sivas Basin likely related to the retreat of an epicontinental sea (Pichat, 2017).

9.3. Implications for the Late Cretaceous to Paleogene Evolution of Central to Eastern Anatolia

Long-lived debate remains about the Late Cretaceous to Paleogene deformation in the Eastern Tauride domain. Based on our observations combined with the recent literature, we propose a scenario regarding the Central to Eastern Anatolia evolution in relation with the closure of northern Neotethys from late Cretaceous onward.

Based on our study and previous interpretations of other ophiolites from the Tauride (e.g., Dilek et al., 1999; Parlak, Çolakoğlu, et al., 2013), Central Anatolia (e.g., van Hinsbergen et al., 2016; Yalınız et al., 2000), and Eastern Anatolia (e.g., Hässig et al., 2015; Rolland et al., 2011), we propose that the Sivas ophiolite was formed in a supra subduction zone setting around ~90–95 Ma, eastward of the Kırşehir (Figure 15a). We suggest that the Sivas ophiolite represents fragments of an oceanic domain that developed in a forearc setting. This oceanic domain was likely characterized by large exposure of serpentinized mantle in relation with the occurrence of extensional detachment fault associated with low magmatic supply. Contemporaneous to possible forearc hyper extension and suprasubduction zone spreading, the lower plate and the northern edge of the Tauride are progressively subducted subsequently, associated with a regional obduction event during the Late Cretaceous (Figure 15b). Frontward of the obducted ophiolitic nappe, accretionary mélange is imbricated, forming later the basement of the Hekimhan and Darende Basins (Booth et al., 2013; Booth et al., 2014). This ophiolitic mélange is probably thinner to the north, or locally absent, such as in the Sivas area. In central Anatolia to the east of the EKFZ (see Gürer & van Hinsbergen, 2018; Gürer, Plunder, et al., 2018; Gürer, van Hinsbergen, et al., 2018), the northernmost part of the Tauride and the whole Kırşehir block were subducted during the Late Cretaceous. Subduction of the Kırşehir block is supported by the HT/LP metamorphism estimated at 800 °C/8 kbar at ~85–90 Ma (Whitney & Hamilton, 2004), prior to its exhumation at ~80–75 Ma (Lefebvre et al., 2013, and references therein).

The Maastrichtian time corresponds to the initiation of supraophiolite sedimentary basins, shortly after obduction (Figure 15c). The most distal part of the Tauride, exposed to the southwest of the Sivas Basin, underwent blueschist facies metamorphism (10 kbar/375 °C, Pourteau et al., 2014). It records peak metamorphism and burial around ~65 Ma before its exhumation (Pourteau et al., 2013). In the Sivas Basin, this period corresponds to the deposition of the Tecer Formation above the Eastern Tauride in the south and deep marine deposits in the trench in the north. This relative uplift of the ophiolite near shallow-water environment reflects probable accretion of the Tauride margin below the ophiolite nappe, such as in Ulukışla further west at the same time (Gürer, Plunder, et al., 2018). Pre-Eocene south verging thrusts and interleaved ophiolites with Tauride Mesozoic carbonates to the south of the Sivas Basin likely highlight this post-obduction accretionary system (Robertson, Parlak, Metin, et al., 2013; Robertson, Parlak, Ustaömer, et al., 2013).

The deformation during latest Paleocene to early Eocene was possibly associated with the exhumation of the northern edge of the Tauride (Afyon zone) and to the Kırşehir block rotation approaching from the

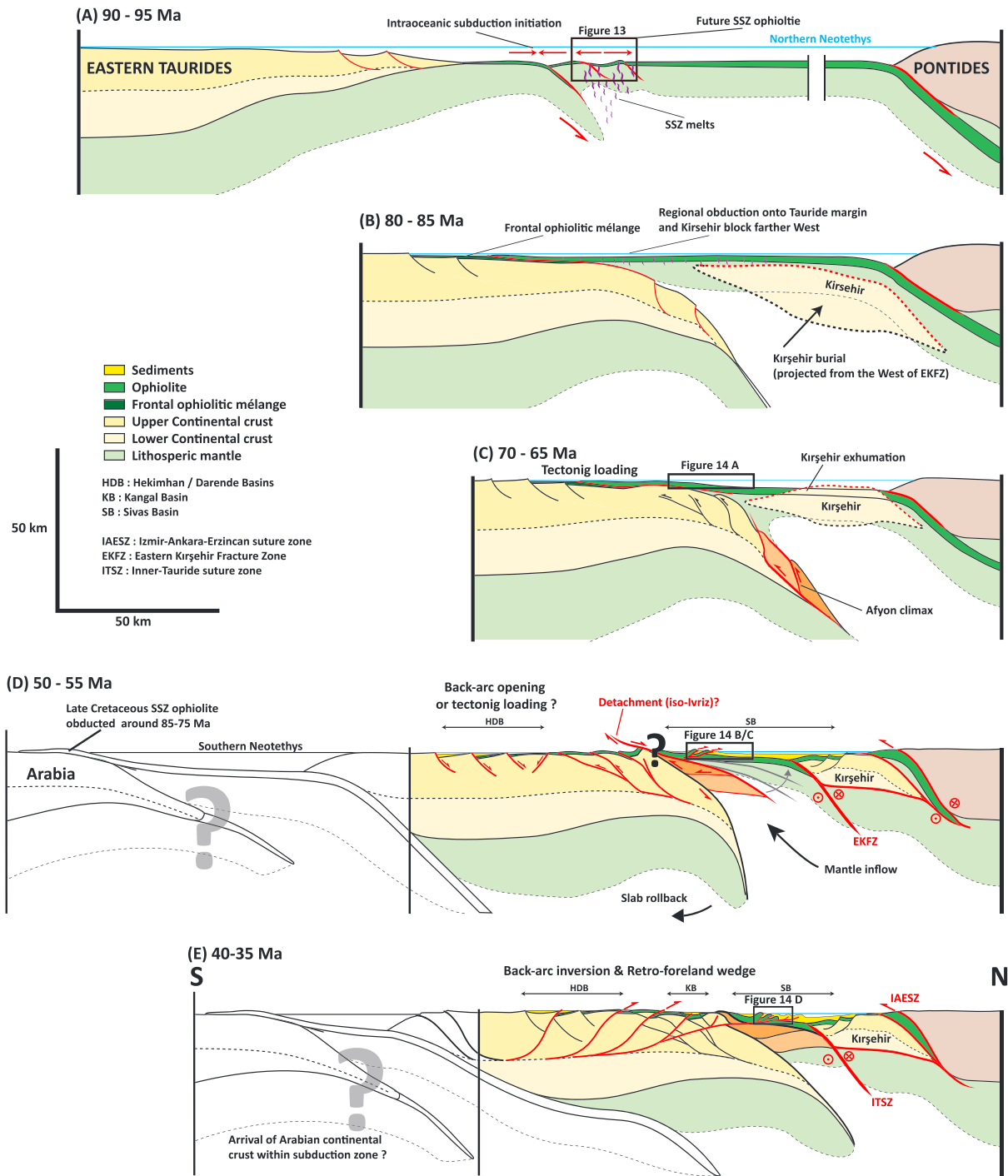


Figure 15. Schematic kinematic scenario integrating the Sivas Basin within a regional geodynamic evolution (see section 9 for details). (a) The Late Cretaceous period is characterized by extension and seafloor spreading in a suprasubduction zone setting, (b) regional obduction over both Kirsehir block and the Tauride, (c) Maastrichtian time is characterized by subduction climax of the northern Tauride and exhumation of Kirsehir block contemporaneous to carbonate platform deposition, and (d) the early Eocene compressive stage may be associated with synexhumation detachment fault in the Ulukışla Basin (Gürer, Plunder, et al., 2018). (e) The middle Eocene to present-day compression in the Sivas Basin resulted from the collision between Tauride and Arabia further to the South.

future collision zone (Figure 15d). In Central Anatolia, exhumation was related to the extensional regime described in Ulukışla Basin and accommodated by the Ivriz detachment (Gürer, Plunder, et al., 2018). Assuming a late Eocene initiation of the Central Anatolian Fault Zone that disconnect the Ulukışla Basin from the Sivas Basin (e.g., Dirik, 2001; Koçyiğit & Beyhan, 1998; Umhoefer et al., 2007), this

regional detachment must be located along the southern edge of the Sivas Basin and therefore associated with extensional structures. However, no equivalent extensional structures have been described within the Sivas Basin in Paleocene and early Eocene sedimentary sequences. In contrast, we documented an early Eocene compressional stage along the southernmost border of the Sivas Basin associated with the reworking of the carbonates from the Tauride platform in the Yağmurluseki Formation (Figure 15d). The cause for such compressional stage remains questionable in the Southern Sivas Basin. Previous studies suggest (e.g., Okay & Sahinturk, 1997) that the late Paleocene to early Eocene compressive stage may result from the collision between the Pontides and the Anatolide-Tauride block. Interestingly, extension within the Hekimhan/Darende Basins during the same period (Figure 15d) has been related either to the subduction of Southern Neotethys below the Eastern Tauride and incipient back-arc opening or to the Eastern Tauride flexure due to loading of crustal-scale south verging fold-and-thrust belt (Booth et al., 2013).

The late Eocene period corresponds to a large-scale regional inversion and emersion (Figure 15e), documented both in the Hekimhan and Darende Basins (Booth et al., 2013; Booth et al., 2014), as well as in the Sivas Basin (Legeay, 2017; Pichat, 2017). This compressional episode is probably related to the initial retrowedge of the Southern Neotethys subduction and incipient Arabia-Tauride collision (e.g., Darin et al., 2018; Legeay, 2017), which was generally assumed to occur during Oligo-Miocene time (e.g. Dhont et al., 2006, Gürer & van Hinsbergen, 2018). The progressive isolation of the Sivas Basin during early to middle Eocene conducted to deposition of a thick evaporite layer dated as 37 Ma (Pichat, 2017). The hypothetical EKFZ will form the future trace of the ITSZ between Taurides and Pontides. Continuous strike-slip motions during Oligo-Miocene resulted in former Central Anatolian Fault zone and associated structures, such as Ecemiş and Deliler-Tecer faults (Jaffey & Robertson, 2001; Yetiş, 1968).

The Oligo-Miocene northward displacement of Arabia and related Eastern Tauride-Arabia collision contributed to progressive rotation of the Eastern Tauride through Oligo-Miocene time. Within the Sivas Basin, it resulted in the progressive development of a fold-and-thrust belt below a thick evaporite layer, involving several generations of salt-related minibasins above (e.g., Kergaravat et al., 2016, 2017; Legeay, Pichat, et al., 2019).

10. Conclusions

By combining field and petrological observations, U-Pb zircon dating, and geochemical analyses, we describe and discuss the pre-obduction to post-obduction evolution of the Sivas ophiolite.

The Sivas ophiolite is made essentially of serpentized mantle with minor mafic intrusions, mostly microgabbro/diorite, troctolite, pegmatitic gabbro, and rodingitized mafic dikes. Most of these intrusions suffered subsequent hydrothermal metamorphism. The top of the serpentized mantle is characterized by an intense brittle deformation and hydrothermal circulation responsible for the formation of ophicalcites. These observations are interpreted as possible evidence for the activity of an extensional detachment fault exhuming the mantle at the seafloor prior to the obduction of the Sivas ophiolite.

New LA-ICP-MS U-Pb zircon analyses for two magmatic intrusions within the serpentized mantle give ages of 91.49 ± 0.8 Ma and 72.7 ± 0.5 Ma. Geochemical analyses from these mafic intrusions indicate a subduction zone influence. All together, field observations, U-Pb zircon dating and geochemical data suggest that the Sivas ophiolite was formed in supra-subduction zone setting during the Late Cretaceous. The younger age is interpreted as a late magmatic event, commonly described in metamorphic soles of Anatolian ophiolites.

The post-obduction sedimentary cover consists of shallow-marine carbonate platforms of Maastrichtian to Paleocene age, followed by massive clastic sedimentation during the early to late Eocene. The field observations combined with first order tectonic calendar highlight tectonic emplacement of ophiolitic thrust sheets along the southern border of the Sivas Basin since early Eocene time. Synkinematic erosion and sedimentation of the southern edge of the Sivas Basin is demonstrated by successive reworking of the ophiolite and of the Late Cretaceous to early Eocene deposits through time toward the north in the Sivas Basin. All these observations are integrated into a conceptual model aiming to reconcile the main tectonic events of Central to Eastern Anatolia.

Acknowledgments

This work results from a research agreement between TOTAL and University of Pau and Pays Adour. Sivas Cumhuriyet University, most particularly H. Temiz, is thanked for support and collaboration during the fieldwork. Mary Ford (University of Lorraine) is warmly thanked for comments. We thank Josep-Serra Kiel (University of Barcelona) and Jérémie Gaillot (Total, CSTJF) for identifying Maastrichtian-Paleocene microfossil and interesting discussions on Late Cretaceous evolution of the basin. Othmar Müntener (University of Lausanne), Jaume Vergés (University of Barcelona) are thanked for fruitful discussions. We also acknowledge the field party: C. Kergaravat, A. Pichat, C. Ribes, C. Bonnel, and B. Rouby (University of Pau). Benoît Petri is thanked for his help for the use of Isoplot software. The authors acknowledge the details reviews by M. Maffione, A. Okay, D. van Hinsbergen, and two anonymous reviewers. Eventually, the Associate Editor F. Rossetti is thanked for his comments as well as the Editor Laurent Jolivet for his advice. Geochemistry and U-Pb dating are presented in their entirety in both manuscript and in the supporting information. Tectonosedimentary data can be obtained from cited references.

References

- Aktimur, H., Tekirli, M., & Yurdakul, M. (1990). Geology of the Sivas-Erzincan Tertiary basin. *Bulletin of the Mineral Research and Exploration Institute of Turkey, Ankara*, 111, 21–30.
- Akyuz, H. S., Ucakus, G., Altunel, E., Dogan, B., & Dikbas, A. (2013). Paleoseismological investigations on a slow-moving active fault in central Anatolia, Tecer Fault, Sivas. *Annals of Geophysics*, 55(5), 847–857. <https://doi.org/10.4401/ag-5444>
- Artan, U., & Sestini, G. (1971). Geology of the Beypinari-Karababa area (Sivas province). *Bulletin Mineral Research and Exploration (Ankara, Turkey)*, 76, 72–89.
- Artemyev, D., & Zaykov, V. (2010). The types and genesis of ophicalcites in lower Devonian olistostromes at cobalt-bearing massive sulfide deposits in the West Magnitogorsk paleoisland arc (South Urals). *Russian Geology and Geophysics*, 51(7), 750–763. <https://doi.org/10.1016/j.rgg.2010.06.003>
- Baykal, F. (1945). Darende ile Kayseri arasındaki Toroslar'ın jeolojik yapısı, İst. Üniv. Fen Fak. Bull(s B).
- Bilgiç, T. (2002). Geological map of Turkey in 1/500.000 scale: Sivas sheet, *Publication of Mineral Research and Exploration Directorate of Turkey (MTA), Ankara*.
- Bogoch, R. (1987). Classification and genetic models of ophicalcites rocks. *Ofoliti*, 12(1), 23–36.
- Booth, M. G., Robertson, A. H., Tasli, K., & Inan, N. (2014). Late Cretaceous to Late Eocene Hekimhan Basin (Central Eastern Turkey) as a supra-ophiolite sedimentary/magmatic basin related to the later stages of closure of Neotethys. *Tectonophysics*, 635, 6–32. <https://doi.org/10.1016/j.tecto.2014.05.039>
- Booth, M. G., Robertson, A. H., Tasli, K., Inan, N., Ünlügenç, U. C., & Vincent, S. (2013). Two-stage development of the Late Cretaceous to Late Eocene Darende Basin: implications for closure of Neotethys in central eastern Anatolia (Turkey). *Geological Society, London, Special Publications*, 372(1), 385–419. <https://doi.org/10.1144/SP372.8>
- Callot, J. P., Ribes, C., Kergaravat, C., Bonnel, C., Temiz, H., Poisson, A., et al. (2014). Salt tectonics in the Sivas basin (Turkey): Crossing salt walls and minibasins. *Bulletin de la Societe Geologique de France*, 185(1), 33–42. <https://doi.org/10.2113/gssgfbull.185.1.33>
- Cannat, M., Bideau, D., & Bougault, H. (1992). Serpentinized peridotites and gabbros in the Mid-Atlantic Ridge axial valley at 15 37' N and 16 52' N. *Earth and Planetary Science Letters*, 109(1-2), 87–106. [https://doi.org/10.1016/0012-821X\(92\)90076-8](https://doi.org/10.1016/0012-821X(92)90076-8)
- Cannat, M., Sauter, D., Mendel, V., Ruellan, E., Okino, K., Escartin, J., et al. (2006). Modes of seafloor generation at a melt-poor ultraslow-spreading ridge. *Geology*, 34(7), 605–608. <https://doi.org/10.1130/G22486.1>
- Cater, J., Hanna, S., Ries, A., & Turner, P. (1991). Tertiary evolution of the Sivas Basin, central Turkey. *Tectonophysics*, 195(1), 29–46. [https://doi.org/10.1016/0040-1951\(91\)90142-F](https://doi.org/10.1016/0040-1951(91)90142-F)
- Çelik, Ö. F., Marzoli, A., Marschik, R., Chiaradia, M., Neubauer, F., & Öz, İ. (2011). Early–Middle Jurassic intra-oceanic subduction in the İzmir-Ankara-Erzincan Ocean, Northern Turkey. *Tectonophysics*, 509(1-2), 120–134. <https://doi.org/10.1016/j.tecto.2011.06.007>
- Clerc, C., Boulvais, P., Lagabrielle, Y., & De Saint Blanquat, M. (2014). Ophicalcites from the northern Pyrenean belt: A field, petrographic and stable isotope study. *International Journal of Earth Sciences*, 103(1), 141–163. <https://doi.org/10.1007/s00531-013-0927-z>
- Darin, M., Umhoefer, P., & Thomson, S. (2018). Rapid late Eocene exhumation of the Sivas Basin (Central Anatolia) driven by initial Arabia-Eurasia collision. *Tectonics*, 37(10), 3805–3833. <https://doi.org/10.1029/2017TC004954>
- Dercourt, J., Zonenshain, L., Ricou, L.-E., Kazmin, V., Le Pichon, X., Knipper, A., et al. (1986). Geological evolution of the Tethys belt from the Atlantic to the Pamirs since the Lias. *Tectonophysics*, 123(1-4), 241–315. [https://doi.org/10.1016/0040-1951\(86\)90199-X](https://doi.org/10.1016/0040-1951(86)90199-X)
- Dhont, D., Chorowicz, J., & Luxey, P. (2006). Anatolian escape tectonics driven by Eocene crustal thickening and Neogene–Quaternary extensional collapse in the eastern Mediterranean region. *Geological Society of America Special Papers*, 409, 441–462. [https://doi.org/10.1130/2006.2409\(21\)](https://doi.org/10.1130/2006.2409(21))
- Dilek, Y., & Furnes, H. (2009). Structure and geochemistry of Tethyan ophiolites and their petrogenesis in subduction rollback systems. *Lithos*, 113(1-2), 1–20. <https://doi.org/10.1016/j.lithos.2009.04.022>
- Dilek, Y., & Furnes, H. (2014). Ophiolites and their origins. *Elements*, 10(2), 93–100. <https://doi.org/10.2113/gselements.10.2.93>
- Dilek, Y., Furnes, H., & Shallo, M. (2007). Suprasubduction zone ophiolite formation along the periphery of Mesozoic Gondwana. *Gondwana Research*, 11(4), 453–475. <https://doi.org/10.1016/j.gr.2007.01.005>
- Dilek, Y., Thy, P., Hacker, B., & Grundvig, S. (1999). Structure and petrology of Tauride ophiolites and mafic dike intrusions (Turkey): Implications for the Neotethyan ocean. *Geological Society of America Bulletin*, 111(8), 1192–1216. [https://doi.org/10.1130/0016-7606\(1999\)111<1192:SAPOTO>2.3.CO;2](https://doi.org/10.1130/0016-7606(1999)111<1192:SAPOTO>2.3.CO;2)
- Dirik, K. (2001). Neotectonic evolution of the northwestward arched segment of the Central Anatolian Fault Zone, Central Anatolia, Turkey. *Geodinamica Acta*, 14(1-3), 147–158. <https://doi.org/10.1080/09853111.2001.11432440>
- Gökten, E. (1983). Şarkışla (Sivas) güney-güneydoğusunun stratigrafisi ve jeolojik evrimi [Stratigraphy and geological evolution of the southsoutheast of Şarkışla]. *Türkiye Jeoloji Kurumu Bülteni*, 26, 167–176.
- Göncüoğlu, M., Turhan, N., & Tekin, U. K. (2003). Evidence for the Triassic rifting and opening of the Neotethyan İzmir-Ankara Ocean and discussion on the presence of Cimmerian events at the northern edge of the Tauride-Anatolide Platform, Turkey. *Bulletin Geological Society Special Publication*, 2, 203–212.
- Görür, N., Oktay, F., Seymen, İ., & Şengör, A. (1984). Palaeotectonic evolution of the Tuzgözü basin complex, Central Turkey: sedimentary record of a Neo-Tethyan closure. *Geological Society, London, Special Publications*, 17(1), 467–482. <https://doi.org/10.1144/GSL.SP.1984.017.01.34>
- Guezou, J.-C., Temiz, H., Poisson, A., & Gürsoy, H. (1996). Tectonics of the Sivas basin: The Neogene record of the Anatolian accretion along the inner Tauric suture. *International Geology Review*, 38(10), 901–925. <https://doi.org/10.1080/00206819709465371>
- Gürer, D., Hinsbergen, D. J., Matenco, L., Corfu, F., & Cascella, A. (2016). Kinematics of a former oceanic plate of the Neotethys revealed by deformation in the Ulukışla basin (Turkey). *Tectonics*, 35, 2385–2416. <https://doi.org/10.1002/2016TC004206>
- Gürer, D., Plunder, A., Kirst, F., Corfu, F., Schmid, S. M., & van Hinsbergen, D. J. (2018). A long-lived Late Cretaceous–early Eocene extensional province in Anatolia? Structural evidence from the Ivri Detachment, southern central Turkey. *Earth and Planetary Science Letters*, 481, 111–124. <https://doi.org/10.1016/j.epsl.2017.10.008>
- Gürer, D., & van Hinsbergen, D. J. (2018). Diachronous demise of the Neotethys Ocean as a driver for non-cylindrical orogenesis in Anatolia. *Tectonophysics*.
- Gürer, D., van Hinsbergen, D. J., Özkaplan, M., Creton, I., Koymans, M. R., Cascella, A., & Langerreis, C. G. (2018). Paleomagnetic constraints on the timing and distribution of Cenozoic rotations in Central and Eastern Anatolia. *Solid Earth*, 9(2), 295–322. <https://doi.org/10.5194/se-9-295-2018>

- Gutnic, M. (1979). *Géologie des taurides occidentales (Turquie)*. Paris: Société géologique de France.
- Hässig, M., Rolland, Y., & Sossou, M. (2015). From seafloor spreading to obduction: Jurassic–Cretaceous evolution of the northern branch of the Neotethys in the Northeastern Anatolian and Lesser Caucasus regions. *Geological Society, London, Special Publications*, 428, 41–60. <https://doi.org/10.1144/SP428.10>
- Hastie, A. R., Kerr, A. C., Pearce, J. A., & Mitchell, S. (2007). Classification of altered volcanic island arc rocks using immobile trace elements: development of the Th–Co discrimination diagram. *Journal of Petrology*, 48(12), 2341–2357. <https://doi.org/10.1093/petrology/egm062>
- Ildefonse, B., Blackman, D. K., John, B. E., Ohara, Y., Miller, D. J., & MacLeod, C. J. (2007). Oceanic core complexes and crustal accretion at slow-spreading ridges. *Geology*, 35(7), 623–626. <https://doi.org/10.1130/G23531A.1>
- İnan, S., & İnan, N. (1990). The features of Gürlevik limestone and a newly suggested name in Tecer formation. *Bulletin of Turkish Geological Society*, 15, 406–417.
- Jaffey, N., & Robertson, A. H. (2001). New sedimentological and structural data from the Ecemiş Fault Zone, southern Turkey: implications for its timing and offset and the Cenozoic tectonic escape of Anatolia. *Journal of the Geological Society*, 158(2), 367–378. <https://doi.org/10.1144/jgs.158.2.367>
- Karacabey, N. (1972). Quelques rudistes provenant de la région de Divriği (Turquie orientale). *Bulletin of the Mineral Research and Exploration*, 78, 46–54.
- Kavak, K. Ş., Parlak, O., & Temiz, H. (2017). Geochemical characteristics of ophiolitic rocks from the southern margin of the Sivas basin and their implications for the Inner Tauride Ocean, Central-Eastern Turkey. *Geodinamica Acta*, 29(1), 160–180. <https://doi.org/10.1080/09853111.2017.1359773>
- Kavak, K. S., Poisson, A., & Guezou, J. C. (1997). Tectonostratigraphy of the Southern Sivas Tertiary Basin (Central Turkey) and Comparison with Landsat MSS Imagery. *International Geology Review*, 39(4), 353–364. <https://doi.org/10.1080/00206819709465277>
- Kaymakçı, N., Ineöz, M., Ertepinar, P., & Koç, A. (2010). Late Cretaceous to recent kinematics of SE Anatolia (Turkey). *Geological Society, London, Special Publications*, 340(1), 409–435. <https://doi.org/10.1144/SP340.18>
- Kergaravat, C. (2016). Dynamique de formation et de déformation de minibassins en contexte compressif: Exemple du bassin de Sivas, Turquie Approche terrain et implications structurales multiéchelles, PhD Thesis (University of Pau, France).
- Kergaravat, C., C. Ribes, J.-P. Callot, C. Bonnel, and J.-C. Ringenbach (2013), Salt tectonics in the Sivas basin, Turkey, mini basin development, halokinetic sequences, and fracturation, paper presented at EGU General Assembly Conference Abstracts.
- Kergaravat, C., Ribes, C., Callot, J. P., & Ringenbach, J. C. (2017). Tectono-stratigraphic evolution of salt-controlled minibasins in a fold and thrust belt, the Oligo-Miocene Sivas Basin, Turkey. *Journal of Structural Geology*, 102, 75–97. <https://doi.org/10.1016/j.jsg.2017.07.007>
- Kergaravat, C., Ribes, C., Legeay, E., Callot, J.-P., Kavak, K., & Ringenbach, J.-C. (2016). Minibasins and salt canopy in foreland fold-and-thrust belts: The central Sivas Basin, Turkey. *Tectonics*, 35, 1342–1366. <https://doi.org/10.1002/2016TC004186>
- Koçyiğit, A., & Beyhan, A. (1998). A new intracontinental transcurrent structure: The Central Anatolian Fault Zone, Turkey. *Tectonophysics*, 284(3–4), 317–336. [https://doi.org/10.1016/S0040-1951\(97\)00176-5](https://doi.org/10.1016/S0040-1951(97)00176-5)
- Kurtman, F. (1973). Geologic and tectonic structure of the Sivas-Hafik-Zara and Imranlı Region. *Bulletin Mineral Research and Exploration (Ankara, Turkey)*, 80, 1–32.
- Lefebvre, C., Barnhoorn, A., van Hinsbergen, D. J., Kaymakçı, N., & Vissers, R. L. (2011). Late Cretaceous extensional denudation along a marble detachment fault zone in the Kırşehir massif near Kaman, central Turkey. *Journal of Structural Geology*, 33(8), 1220–1236. <https://doi.org/10.1016/j.jsg.2011.06.002>
- Lefebvre, C., Meijers, M. J., Kaymakçı, N., Peynircioğlu, A., Langereis, C. G., & van Hinsbergen, D. J. (2013). Reconstructing the geometry of central Anatolia during the late Cretaceous: Large-scale Cenozoic rotations and deformation between the Pontides and Taurides. *Earth and Planetary Science Letters*, 366, 83–98. <https://doi.org/10.1016/j.epsl.2013.01.003>
- Legeay, E. (2017). Géodynamique du Bassin de Sivas (Turquie)—De la fermeture d'un domaine océanique à la mise en place d'un avant-pays salifère, PhD Thesis (University of Pau, France).
- Legeay, E., Pichat, A., Kergaravat, C., Ribes, C., Callot, J.-P., Ringenbach, J.-C., et al. (2019). Geology of the Central Sivas Basin (Turkey). *Journal of Maps*, 15(2), 406–417. <https://doi.org/10.1080/17445647.2018.1514539>
- Legeay, E., Ringenbach, J. C., Kergaravat, C., Pichat, A., Mohn, G., Vergés, J., et al. (2019). Structure and kinematics of the Central Sivas Basin (Turkey): Salt deposition and tectonics in an evolving fold-and-thrust belt. *Geological Society, London, Special Publications*, 490, SP490-2019-92. <https://doi.org/10.1144/SP490-2019-92>
- Lemoine, M., Tricart, P., & Boillot, G. (1987). Ultramafic and gabbroic ocean floor of the Ligurian Tethys (Alps, Corsica, Apennines): In search of a genetic imodel. *Geology*, 15(7), 622–625. [https://doi.org/10.1130/0091-7613\(1987\)15<622:UAGOFO>2.0.CO;2](https://doi.org/10.1130/0091-7613(1987)15<622:UAGOFO>2.0.CO;2)
- Ludwig, K. R. (2012). *Isoplot 3.75–4.15: A geochronological toolkit for Microsoft Excel*, Berkeley Geochronology Center Special Publication, Berkeley, California.
- Mackintosh, P. W., & Robertson, A. H. (2009). Structural and sedimentary evidence from the northern margin of the Tauride platform in south central Turkey used to test alternative models of Tethys during Early Mesozoic time. *Tectonophysics*, 473(1–2), 149–172. <https://doi.org/10.1016/j.tecto.2008.10.031>
- Mackintosh, P. W., & Robertson, A. H. (2012). Late Devonian–Late Triassic sedimentary development of the central Taurides, S Turkey: Implications for the northern margin of Gondwana. *Gondwana Research*, 21(4), 1089–1114. <https://doi.org/10.1016/j.gr.2011.07.016>
- Maffione, M., Hinsbergen, D. J., Gelder, G. I., Goes, F. C., & Morris, A. (2017). Kinematics of Late Cretaceous subduction initiation in the Neo-Tethys Ocean reconstructed from ophiolites of Turkey, Cyprus, and Syria. *Journal of Geophysical Research: Solid Earth*, 122, 3953–3976. <https://doi.org/10.1002/2016JB013821>
- Maffione, M., Thieulot, C., van Hinsbergen, D. J., Morris, A., Plümper, O., & Spakman, W. (2015). Dynamics of intraoceanic subduction initiation: 1. Oceanic detachment fault inversion and the formation of supra-subduction zone ophiolites. *Geochemistry, Geophysics, Geosystems*, 16, 1753–1770. <https://doi.org/10.1002/2015GC005746>
- Maffione, M., van Hinsbergen, D. J., Koornneef, L. M., Guilmette, C., Hodges, K., Borneman, N., et al. (2015). Forearc hyperextension dismembered the south Tibetan ophiolites. *Geology*, 43(6), 475–478. <https://doi.org/10.1130/G36472.1>
- Menant, A., Jolivet, L., & Vrielynck, B. (2016). Kinematic reconstructions and magmatic evolution illuminating crustal and mantle dynamics of the eastern Mediterranean region since the late Cretaceous. *Tectonophysics*, 675, 103–140. <https://doi.org/10.1016/j.tecto.2016.03.007>
- Metcalfe, R. V., & Shervais, J. W. (2008). Suprasubduction-zone ophiolites: Is there really an ophiolite conundrum? In *Geological Society of America Special Papers*, (Vol. 438, pp. 191–222). Boulder, Colo.: Geological Society of America.

- Morris, A., Anderson, M. W., Omer, A., Maffione, M., & van Hinsbergen, D. J. (2017). Rapid fore-arc extension and detachment-mode spreading following subduction initiation. *Earth and Planetary Science Letters*, 478, 76–88. <https://doi.org/10.1016/j.epsl.2017.08.040>
- Okay, A. I. (2008). Geology of Turkey: A synopsis. *Der Anschnitt*, 21, 19–42.
- Okay, A. I., & Altıner, D. (2007). A condensed Mesozoic succession north of İzmir: A fragment of the Anatolide-Tauride platform in the Bornova Flysch Zone. *Turkish Journal of Earth Sciences*, 16(3), 257–279.
- Okay, A. I., & Nikishin, A. M. (2015). Tectonic evolution of the southern margin of Laurasia in the Black Sea region. *International Geology Review*, 57(5-8), 1051–1076. <https://doi.org/10.1080/00206814.2015.1010609>
- Okay, A. I., & Sahintürk, Ö. (1997). Geology of the Eastern Pontides. In A. G. Robinson (Ed.), *Regional and Petroleum Geology of the Black Sea and Surrounding Region, American Association of Petroleum Geologists Memoir* (Vol. 68, pp. 291–311).
- Özgül, N. (1984). Stratigraphy and tectonic evolution of the Central Taurides. In *Geology of the Taurus belt*, (pp. 77–90). Ankara, Turkey: MTA.
- Parlak, O., Çolakoğlu, A., Dönmez, C., Sayak, H., Yildirim, N., Türkel, A., & Odabaşı, İ. (2013). Geochemistry and tectonic significance of ophiolites along the İzmir–Ankara–Erzincan Suture Zone in northeastern Anatolia. *Geological Society, London, Special Publications*, 372(1), 75–105. <https://doi.org/10.1144/SP372.7>
- Parlak, O., Karaoğlu, F., Rızaoğlu, T., Klötzli, U., Koller, F., & Billor, Z. (2013). U–Pb and 40 Ar–39 Ar geochronology of the ophiolites and granitoids from the Tauride belt: Implications for the evolution of the Inner Tauride suture. *Journal of Geodynamics*, 65, 22–37. <https://doi.org/10.1016/j.jog.2012.06.012>
- Parlak, O., Yılmaz, H., & Boztuğ, D. (2006). Origin and tectonic significance of the metamorphic sole and isolated dykes of the Divriği ophiolite (Sivas, Turkey): Evidence for slab break-off prior to ophiolite emplacement. *Turkish Journal of Earth Sciences*, 15(1), 25–45.
- Pearce, J. A. (2003). *Supra-subduction zone ophiolites: The search for modern analogues, Special Papers-Geological Society of America*, (pp. 269–294). USA: Geological Society of America.
- Pearce, J. A. (2008). Geochemical fingerprinting of oceanic basalts with applications to ophiolite classification and the search for Archean oceanic crust. *Lithos*, 100(1-4), 14–48. <https://doi.org/10.1016/j.lithos.2007.06.016>
- Pearce, J. A., & Norry, M. J. (1979). Petrogenetic implications of Ti, Zr, Y, and Nb variations in volcanic rocks. *Contributions to Mineralogy and Petrology*, 69(1), 33–47. <https://doi.org/10.1007/BF00375192>
- Péron-Pinvidic, G., & Manatschal, G. (2009). The final rifting evolution at deep magma-poor passive margins from Iberia-Newfoundland: A new point of view. *International Journal of Earth Sciences*, 98(7), 1581–1597. <https://doi.org/10.1007/s00531-008-0337-9>
- Pichat, A. (2017). Dynamique des systèmes évaporitiques d'un bassin d'avant-pays salifère et processus diagénétiques associés au contexte halocinétique: Exemple du bassin de Sivas en Turquie, *PhD Thesis (University of Pau, France)*.
- Pichat, A., Callot, J.-P., & Ringenbach, J.-C. (2016). Diagenesis of Oligocene continental sandstones in salt-walled mini-basins—Sivas Basin, Turkey. *Sedimentary Geology*, 339, 13–31. <https://doi.org/10.1016/j.sedgeo.2016.03.025>
- Pichat, A., Hoareau, G., Callot, J. P., Legeay, E., Kavak, K. S., Révillon, S., et al. (2018). Evidence of multiple evaporite recycling processes in a salt-tectonic context, Sivas Basin, Turkey. *Terra Nova*, 30(1), 40–49. <https://doi.org/10.1111/ter.12306>
- Plunder, A., Agard, P., Chopin, C., Pourteau, A., & Okay, A. I. (2015). Accretion, underplating and exhumation along a subduction interface: From subduction initiation to continental subduction (Tavşanlı zone, W. Turkey). *Lithos*, 226, 233–254. <https://doi.org/10.1016/j.lithos.2015.01.007>
- Poisson, A. (1977). Recherches géologiques dans les Taurides occidentales (Turquie), Université de Paris-Sud (Centre D'orsay).
- Poisson, A., Guezou, J.-C., Ozturk, A., İnan, S., Temiz, H., Gürsöy, H., et al. (1996). Tectonic setting and evolution of the Sivas Basin, central Anatolia, Turkey. *International Geology Review*, 38(9), 838–853. <https://doi.org/10.1080/00206819709465366>
- Poisson, A., Vrielynck, B., Wernli, R., Negri, A., Bassetti, M.-A., Büyükermerç, Y., et al. (2016). Miocene transgression in the central and eastern parts of the Sivas Basin (Central Anatolia, Turkey) and the Cenozoic palaeogeographical evolution. *International Journal of Earth Sciences*, 105(1), 339–368. <https://doi.org/10.1007/s00531-015-1248-1>
- Pourteau, A., Bousquet, R., Vidal, O., Plunder, A., Duesterhoeft, E., Candan, O., & Oberhänsli, R. (2014). Multistage growth of Fe–Mg–carpholite and Fe–Mg–chloritoid, from field evidence to thermodynamic modelling. *Contributions to Mineralogy and Petrology*, 168(6), 1090. <https://doi.org/10.1007/s00410-014-1090-7>
- Pourteau, A., Candan, O., & Oberhänsli, R. (2010). High-pressure metasediments in central Turkey: Constraints on the Neotethyan closure history. *Tectonics*, 29, TC5004. <https://doi.org/10.1029/2009TC002650>
- Pourteau, A., Sudo, M., Candan, O., Lanari, P., Vidal, O., & Oberhänsli, R. (2013). Neotethys closure history of Anatolia: insights from ⁴⁰Ar–³⁹Ar geochronology and P–T estimation in high-pressure metasedimentary rocks. *Journal of Metamorphic Geology*, 31(6), 585–606. <https://doi.org/10.1111/jmg.12034>
- Ribes, C. (2015). Interaction entre la tectonique salifère et la sédimentation dans des mini-bassins: Exemple de l'Oligo-Miocène du bassin de Sivas, Turquie, *PhD Thesis (University of Pau, France)*.
- Ribes, C., Kergaravat, C., Bonnel, C., Crumeyrolle, P., Callot, J.-P., Poisson, A., et al. (2015). Fluvial sedimentation in a salt-controlled mini-basin: stratal patterns and facies assemblages, Sivas Basin, Turkey. *Sedimentology*, 62(6), 1513–1545. <https://doi.org/10.1111/sed.12195>
- Ribes, C., Kergaravat, C., Crumeyrolle, P., Lopez, M., Bonnel, C., Poisson, A., et al. (2016). Factors controlling stratal pattern and facies distribution of fluvio-lacustrine sedimentation in the Sivas mini-basins, Oligocene (Turkey). *Basin Research*, 29, 596–621. <https://doi.org/10.1111/bre.12171>
- Ribes, C., Lopez, M., Kergaravat, C., Crumeyrolle, P., Poisson, A., Callot, J.-P., et al. (2018). Facies partitioning and stratal pattern in salt-controlled marine to continental mini-basins: Examples from the late Oligocene to early Miocene of the Sivas Basin, Turkey. *Marine and Petroleum Geology*, 93, 468–496. <https://doi.org/10.1016/j.marpetgeo.2018.03.018>
- Ricou, L. E. (1971). Le croissant ophiolitique péri-arabe: Une ceinture de nappes mises en place au crétacé supérieur. *Géographie Physique et de Géologie Dynamique*, 13, 327–349.
- Ringenbach, J.-C., Salel, J.-F., Kergaravat, C., Ribes, C., Bonnel, C., & Callot, J.-P. (2013). Salt tectonics in the Sivas Basin, Turkey: outstanding seismic analogues from outcrops. *First Break*, 31(6), 93–101. <https://doi.org/10.3997/1365-2397.2013016>
- Robertson, A. H. F. (2002). Overview of the genesis and emplacement of Mesozoic ophiolites in the Eastern Mediterranean Tethyan region. *Lithos*, 65(1-2), 1–67. [https://doi.org/10.1016/S0024-4937\(02\)00160-3](https://doi.org/10.1016/S0024-4937(02)00160-3)
- Robertson, A. H. F. (2004). Development of concepts concerning the genesis and emplacement of Tethyan ophiolites in the Eastern Mediterranean and Oman regions. *Earth-Science Reviews*, 66(3-4), 331–387. <https://doi.org/10.1016/j.earscirev.2004.01.005>
- Robertson, A. H. F., Clift, P., Degnan, P., & Jones, G. (1991). Palaeogeographic and palaeotectonic evolution of the Eastern Mediterranean Neotethys. *Palaeogeography, Palaeoclimatology, Palaeoecology*, 87(1-4), 289–343. [https://doi.org/10.1016/0031-0182\(91\)90140-M](https://doi.org/10.1016/0031-0182(91)90140-M)

- Robertson, A. H. F., Dixon, J., Brown, S., Collins, A., Morris, A., Pickett, E., et al. (1996). Alternative tectonic models for the Late Palaeozoic–Early Tertiary development of Tethys in the Eastern Mediterranean region. *Geological Society, London, Special Publications*, 105(1), 239–263. <https://doi.org/10.1144/GSL.SP.1996.105.01.22>
- Robertson, A. H. F., Parlak, O., Metin, Y., Vergili, Ö., Tasli, K., İnan, N., & Soyacan, H. (2013). Late Palaeozoic–Cenozoic tectonic development of carbonate platform, margin and oceanic units in the Eastern Taurides, Turkey. *Geological Society, London, Special Publications*, 372(1), 167–218. <https://doi.org/10.1144/SP372.16>
- Robertson, A. H. F., Parlak, O., & Ustaömer, T. (2012). Overview of the Palaeozoic–Neogene evolution of Neotethys in the Eastern Mediterranean region (southern Turkey, Cyprus, Syria). *Petroleum Geoscience*, 18(4), 381–404. <https://doi.org/10.1144/petgeo2011-091>
- Robertson, A. H. F., Parlak, O., Ustaömer, T., Tasli, K., İnan, N., Dumitrica, P., & Karaoğlan, F. (2013). Subduction, ophiolite genesis and collision history of Tethys adjacent to the Eurasian continental margin: New evidence from the Eastern Pontides, Turkey. *Geodinamica Acta*, 26(3–4), 230–293. <https://doi.org/10.1080/09853111.2013.877240>
- Rolland, Y., Sosson, M., Adamia, S., & Sadradze, N. (2011). Prolonged Variscan to Alpine history of an active Eurasian margin (Georgia, Armenia) revealed by $^{40}\text{Ar}/^{39}\text{Ar}$ dating. *Gondwana Research*, 20(4), 798–815. <https://doi.org/10.1016/j.gr.2011.05.007>
- Sarıfakıoğlu, E., Özen, H., & Winchester, J. A. (2009). Petrogenesis of the Refahiye ophiolite and its tectonic significance for Neotethyan ophiolites along the İzmir–Ankara–Erzincan suture zone. *Turkish Journal of Earth Sciences*, 18, 187–207.
- Saunders, A. D., Tarney, J., & Weaver, S. D. (1980). Transverse geochemical variations across the Antarctic Peninsula: implications for the genesis of calc-alkaline magmas. *Earth and Planetary Science Letters*, 46(3), 344–360. [https://doi.org/10.1016/0012-821X\(80\)90050-3](https://doi.org/10.1016/0012-821X(80)90050-3)
- Seibold, E., & Berger, W. (2017). *The sea floor: an introduction to marine geology*. Berlin, Heidelberg: Springer. <https://doi.org/10.1007/978-3-319-51412-3>
- Şengör, A., & Yılmaz, Y. (1981). Tethyan evolution of Turkey: A plate tectonic approach. *Tectonophysics*, 75(3–4), 181–241. [https://doi.org/10.1016/0040-1951\(81\)90275-4](https://doi.org/10.1016/0040-1951(81)90275-4)
- Shervais, J. W. (1982). Ti–V plots and the petrogenesis of modern and ophiolitic lavas. *Earth and Planetary Science Letters*, 59(1), 101–118. [https://doi.org/10.1016/0012-821X\(82\)90120-0](https://doi.org/10.1016/0012-821X(82)90120-0)
- Sun, S. S., & McDonough, W. F. (1989). Chemical and isotopic systematics of oceanic basalts: implications for mantle composition and processes. *Geological Society, London, Special Publications*, 42(1), 313–345. <https://doi.org/10.1144/GSL.SP.1989.042.01.19>
- Temiz, H. (1996). Tectonostratigraphy and thrust tectonics of the central and eastern parts of the Sivas Tertiary basin, Turkey. *International Geology Review*, 38(10), 957–971. <https://doi.org/10.1080/00206819709465374>
- Temiz, H., Guezou, J.-C., Poisson, A., & Tutkun, Z. (1993). Tectonostratigraphy and kinematics of the eastern end of the Sivas Basin (central eastern Turkey): Implications for the so-called ‘Anatolian block’. *Geological Journal*, 28(3–4), 239–250. <https://doi.org/10.1002/gj.3350280304>
- Topuz, G., Çelik, Ö. F., Şengör, A. C., Altıntaş, İ. E., Zack, T., Rolland, Y., & Barth, M. (2013). Jurassic ophiolite formation and emplacement as backstop to a subduction-accretion complex in northeast Turkey, the Refahiye ophiolite, and relation to the Balkan ophiolites. *American Journal of Science*, 313(10), 1054–1087. <https://doi.org/10.2475/10.2013.04>
- Umhoefer, P. J., Whitney, D. L., Teyssier, C., Fayon, A. K., Casale, G., & Heizler, M. T. (2007). Yo-yo tectonics in a wrench zone, Central Anatolian fault zone, Turkey. *Geological Society of America Special Papers*, 434, 35–57. [https://doi.org/10.1130/2007.2434\(03\)](https://doi.org/10.1130/2007.2434(03))
- Ustaömer, T. m., & Robertson, A. H. (2010). Late Palaeozoic–Early Cenozoic tectonic development of the Eastern Pontides (Artvin area), Turkey: Stages of closure of Tethys along the southern margin of Eurasia. *Geological Society, London, Special Publications*, 340(1), 281–327. <https://doi.org/10.1144/SP340.13>
- Uysal, I., Ersoy, E. Y., Dilek, Y., Escayola, M., Sarıfakıoğlu, E., Saka, S., & Hirata, T. (2015). Depletion and refertilization of the Tethyan oceanic upper mantle as revealed by the early Jurassic Refahiye ophiolite, NE Anatolia—Turkey. *Gondwana Research*, 27(2), 594–611. <https://doi.org/10.1016/j.gr.2013.09.008>
- van Hinsbergen, D. J., Peters, K., Maffione, M., Spakman, W., Guilmette, C., Thieulot, C., et al. (2015). Dynamics of intraoceanic subduction initiation: 2. Suprasubduction zone ophiolite formation and metamorphic sole exhumation in context of absolute plate motions. *Geochemistry, Geophysics, Geosystems*, 16, 1771–1785. <https://doi.org/10.1002/2015GC005745>
- van Hinsbergen, D. J. J., Maffione, M., Plunder, A., Kaymakçı, N., Ganerød, M., Hendriks, B. W. H., et al. (2016). Tectonic evolution and paleogeography of the Kırşehir Block and the Central Anatolian Ophiolites, Turkey. *Tectonics*, 35, 983–1014. <https://doi.org/10.1002/2015TC004018>
- Whitmarsh, R., Manatschal, G., & Minshull, T. (2001). Evolution of magma-poor continental margins from rifting to seafloor spreading. *Nature*, 413(6852), 150–154. <https://doi.org/10.1038/35093085>
- Whitney, D., Teyssier, C., Dilek, Y., & Fayon, A. (2001). Metamorphism of the Central Anatolian Crystalline Complex, Turkey: Influence of orogen-normal collision vs. wrench-dominated tectonics on P–T–t paths. *Journal of Metamorphic Geology*, 19(4), 411–432. <https://doi.org/10.1046/j.0263-4929.2001.00319.x>
- Whitney, D. L., & Hamilton, M. A. (2004). Timing of high-grade metamorphism in central Turkey and the assembly of Anatolia. *Journal of the Geological Society*, 161(5), 823–828. <https://doi.org/10.1144/0016-764903-081>
- Winchester, J. A., & Floyd, P. A. (1977). Geochemical discrimination of different magma series and their differentiation products using immobile elements. *Chemical Geology*, 20, 325–343. [https://doi.org/10.1016/0009-2541\(77\)90057-2](https://doi.org/10.1016/0009-2541(77)90057-2)
- Wood, D. A. (1980). The application of a Th Hf Ta diagram to problems of tectonomagmatic classification and to establishing the nature of crustal contamination of basaltic lavas of the British Tertiary Volcanic Province. *Earth and Planetary Science Letters*, 50(1), 11–30. [https://doi.org/10.1016/0012-821X\(80\)90116-8](https://doi.org/10.1016/0012-821X(80)90116-8)
- Yalnız, K., & Gönçüoğlu, M. C. (1998). General geological characteristics and distribution of the Central Anatolian Ophiolites. *Yerbilimleri*, 20, 19–30.
- Yalnız, M. K., Gönçüoğlu, M. C., & Oezkan-Altuner, S. (2000). Formation and emplacement ages of the SSZ-type Neotethyan ophiolites in Central Anatolia, Turkey: Palaeotectonic implications. *Geological Journal*, 35(2), 53–68. [https://doi.org/10.1002/1099-1034\(200004/06\)35:2<53::AID-GJ837>3.0.CO;2-6](https://doi.org/10.1002/1099-1034(200004/06)35:2<53::AID-GJ837>3.0.CO;2-6)
- Yetiş, C. (1968). Geology of the Çamardı (Niğde) region and the characteristics of the Ecemiş Fault Zone between Maden Boğazi and Kamlıç. *Istanbul Üniversitesi Fen Fakültesi Mecmuası, Seri B*, 43, 41–61.
- Yılmaz, A., Sumengen, M., Terlemeç, I., & Bilgic, T. (1989). *1: 100 000 Ölçekli Acinsama Nitelikli Türkiye Jeolojisi Haritaları Serisi, Sivas G-23 paftası*. Ankara: MTA Yayını.